RADC-TR-68-125
Final Report

COMPARISON OF MONOPULSE AND MECHANICAL TRACK-WHILE-SCAN RADARS

Charles F. Bough

TECHNICAL REPORT NO. RADC-TR- 68-125
May 1968

Rome Air Development Center
Air Force Systems Command
Griffiss Air Force Base, New York

When US Government drawings, specifications, or other data are used for any purpose other than a definitely related government procurement operation, the government thereby incurs no responsibility nor any obligation whatsoever; and the fact that the government may have formulated, furnished, or in any way supplied the said drawings, specifications, or other data is not to be regarded, by implication or otherwise, as in any manner licensing the holder or any other person or corporation, or conveying any rights or permission to manufacturer, use, or sell any patented invention that may in any way be related thereto.

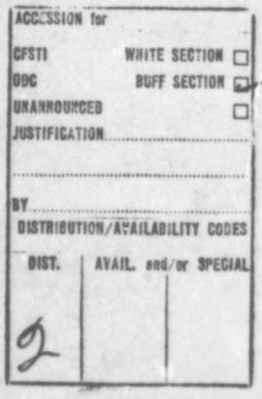

Do not return this copy. Retain or destroy.

COMPARISON OF MONOPULSE AND MECHANICAL TRACK-WHILE-SCAN RADARS

Charles F. Bough

AFLC, GAFB, N.Y., 3 Jun 68-52

FOREWORD

There have not been many applications of electro-mechanical scanners in radar systems, nor any particular striking developments in this field since the advent of electronic scanning techniques. In fact, there have been none since the basic design work done by Foster, Robinson and Lewis.

This technical report has been written to introduce the basic concept of an electro-mechanical track-while-scan radar employing the Lewis Type Scanner and to present it in a clear and simplified manner so it may be easily understood. The report is based, to a great extent, on the experience of the author and will acquaint those people having an engineering background with track-while-scan radar. In order to give the user an intuitive understanding of the design and operation of the track-while-scan radar, a comparison is made with the familiar amplitude monopulse auto tracking radar. The appendices present material on the design theory of the Lewis Scanner (U. S. Pat. No. 2, 585, 562), tracking loop design and an analysis of the tracking loop errors. This material will be of invaluable assistance to engineers who must understand the operation of electro-mechanical track-while-scan radars. The characteristics of this type of system make it very desirable for use as Ground Control Approach radar, especially now when many airports will be using parallel runways in order to handle the increased air traffic.

The author would like to thank Mr. Quentin Porter, who read the manuscript critically and made many helpful suggestions. He is particularly grateful to Mrs. V. Facchino, whose careful checking of the manuscript has removed many errors and to Ellen LaSota who cheerfully retyped the manuscript many times.

PUBLICATION REVIEW

This report has been reviewed and is approved.

Approved: Charles F. Bough
CHARLES F. BOUGH
Chief, Instrumentation Unit
Measurement Section

Approved: Richard M. Cosel
RICHARD M. COSEL
Colonel, USAF
Chief, Communications Division

FOR THE COMMANDER: Irving J. Gabelman
IRVING J. GABELMAN
Chief, Advanced Studies Group

ABSTRACT

This report compares the angle-range tracking capabilities of amplitude monopulse radars and track-while-scan radar using mechanical scanners developed by Lewis (U.S. Patent No. 2, 585, 562). Both systems are described along with an error analysis of the angle-range tracking loops. A table which summarizes the characteristics of the two systems is included.

TABLE OF CONTENTS

Contents	Page
INTRODUCTION	1
DESCRIPTION OF MONOPULSE AND TRACK-WHILE-SCAN SYSTEM	1
COMPARISON OF TWS AND MONOPULSE RADARS	5
RECEIVER AND DETECTORS	5
ANGLE MEASUREMENT ERROR ANALYSIS	5
RANGE MEASUREMENT ERROR ANALYSIS	9
TRACK-WHILE-SCAN RADAR ACCURACY EVALUATION	13
COMPARISON/SUMMARY OF CHARACTERISTICS	18
APPENDIX I - LEWIS SCANNER DESIGN	20
APPENDIX II - TRACKING LOOP DESIGN	26
APPENDIX III - TRACKING LOOP ERRORS - TRACK-WHILE-SCAN	39
REFERENCES	50
LIST OF ABBREVIATIONS AND SYMBOLS	51

LIST OF ILLUSTRATIONS

FIGURE PAGE

1. BLOCK DIAGRAM OF TWO COORDINATE (AZIMUTH AND ELEVATION) AMPLITUDE COMPARISON MONOPULSE SYSTEM..... 2
2. BLOCK DIAGRAM OF TRACK-WHILE-SCAN RADAR SYSTEM (SIMPLIFIED ONE ANGULAR COORDINATE CHANNEL)..... 4
3. FUNCTIONAL DIAGRAM OF ANGLE TRACKING LOOP..... 9
4. TRACKING LOOP BANDWIDTH..... 10
5. SPLIT RANGE GATE TRACKING..... 11
6. RELATIVE CONTRIBUTIONS TO ANGULAR TRACKING ERROR DUE TO AMPLITUDE FLUCTUATIONS, ANGLE FLUCTUATIONS, RECEIVER NOISE," AND SERVO NOISE OF FUNCTION OF RANGE (A) COMPOSITE ERROR FOR CONICAL SCAN (B) FOR TRACK-WHILE-SCAN (C) FOR MONOPULSE... 16

APPENDIX I

1. LEWIS SCANNER, OPTICAL AND PHYSICAL CONSIDERATIONS..... 22
2. LEWIS SCANNER ANTENNA GEOMETRY..... 23
3. LEWIS SCANNER ANTENNA CONFIGURATION..... 24

APPENDIX II

1. TYPE 2 TRACKING LOOPS..... 27
2. TRANSIENT RESPONSE OF TYPE 2 SYSTEM FOR POSITION STEP INPUT 29
3. PASS-COURSE TRACKING PROBLEM..... 30
4. TRACKING LOOP BANDWIDTH..... 32
5. FREQUENCY RESPONSE (ANGLE TRACKING LOOP $\omega_o = 1$) 35
6. CORNER FREQUENCY ω_o FOR R_{max} AT VARIOUS RANGES AND VELOCITIES....37
7. FREQUENCY RESPONSE (RANGE TRACKING LOOP $\omega_o = 4$)..... 38

LIST OF ILLUSTRATIONS (Cont'd)

APPENDIX III

Page

3.1 SPLIT GATE ANGULAR POSITION ESTIMATOR..... 40

3.2 SKETCH SHOWING THE SIGNAL PROCESSING IN THE TRACKING LOOP..... 43

3.3 ANTENNA BEAM SHAPE USED IN THE TRACKING LOOP..... 45

3.4 EFFECT OF "PANT LEG" GATE PARAMETERS ON NORMALIZED TRACKING ACCURACY FOR SCAN ON BOTH TRANSMIT AND RECEIVE..... 46

3.5 EFFECT OF SINGAL-TO-NOSIE RATIO ON TRACKING ACCURACY..... 48

3.6 PULSE PROCESSING EFFICIENCY..... 49

BLANK PAGE

INTRODUCTION

The work reported here is an integral part of an over-all program on tracking radars which began in 1962 as an in-house study. It compares the angle-range tracking capabilities of monopulse radars and track-while-scan (TWS) radars using scanners of the type developed by Foster, Robinson and Lewis.

Any comparison of monopulse and track-while-scan (TWS) radars is made difficult by the variety of configurations employed in both. This report covers the most commonly used four-horn, amplitude comparison monopulse system and the Lewis Scanner, track-while-scan system. Each system will be described and then compared on the following:

- Antenna and RF System
- Receiver/Detector Operation
- Angle/Range Tracking Ability

DESCRIPTION OF MONOPULSE AND TRACK-WHILE SCAN SYSTEM

A tracking radar system measures the coordinates of a target and provides data which may be used to determine the target path and to predict its future position. Although any radar can be considered a tracking radar, the method by which angle tracking is accomplished distinguishes what is normally considered a continuous tracking (monopulse or conical scan) radar from any other radar. It is also necessary to distinguish between the electronic track-while-scan and the mechanical track-while-scan radars. The electro-mechanical track-while-scan radar supplied continuous tracking data on a single target and the electronic (beam steering) track-while-scan supplies sampled tracking data on many targets. This discussion will include the mechanical track-while-scan radars which employ equipment and circuits similar to those used in the conical scan radar systems for angle and range tracking. The basic difference between the monopulse and TWS radars is in the method used to track a target in angle and position the antenna to track the target.

The antenna beam in the monopulse radar is positioned in angle to track a target by a servo mechanism actuated by an error signal, while the TWS uses a scanner reference signal to determine the target position within the scanned sector and generates error signal for a servo mechanism to control the position of the angle gate. These various methods of generating the error signal are classified as simultaneous lobing or monopulse and sequential lobing. In both of these systems, automatic range tracking is accomplished by a servo control loop actuated by an error signal generated in the receiver.

A block diagram of an amplitude comparison monopulse radar with provisions for obtaining error signals in both elevation and azimuth is shown in Figure 1. The most common form of monopulse is the hybrid comparator, where the four feeds generate four partially overlapping antenna beams. Basically, it uses amplitude comparison with the combining done at the feeds

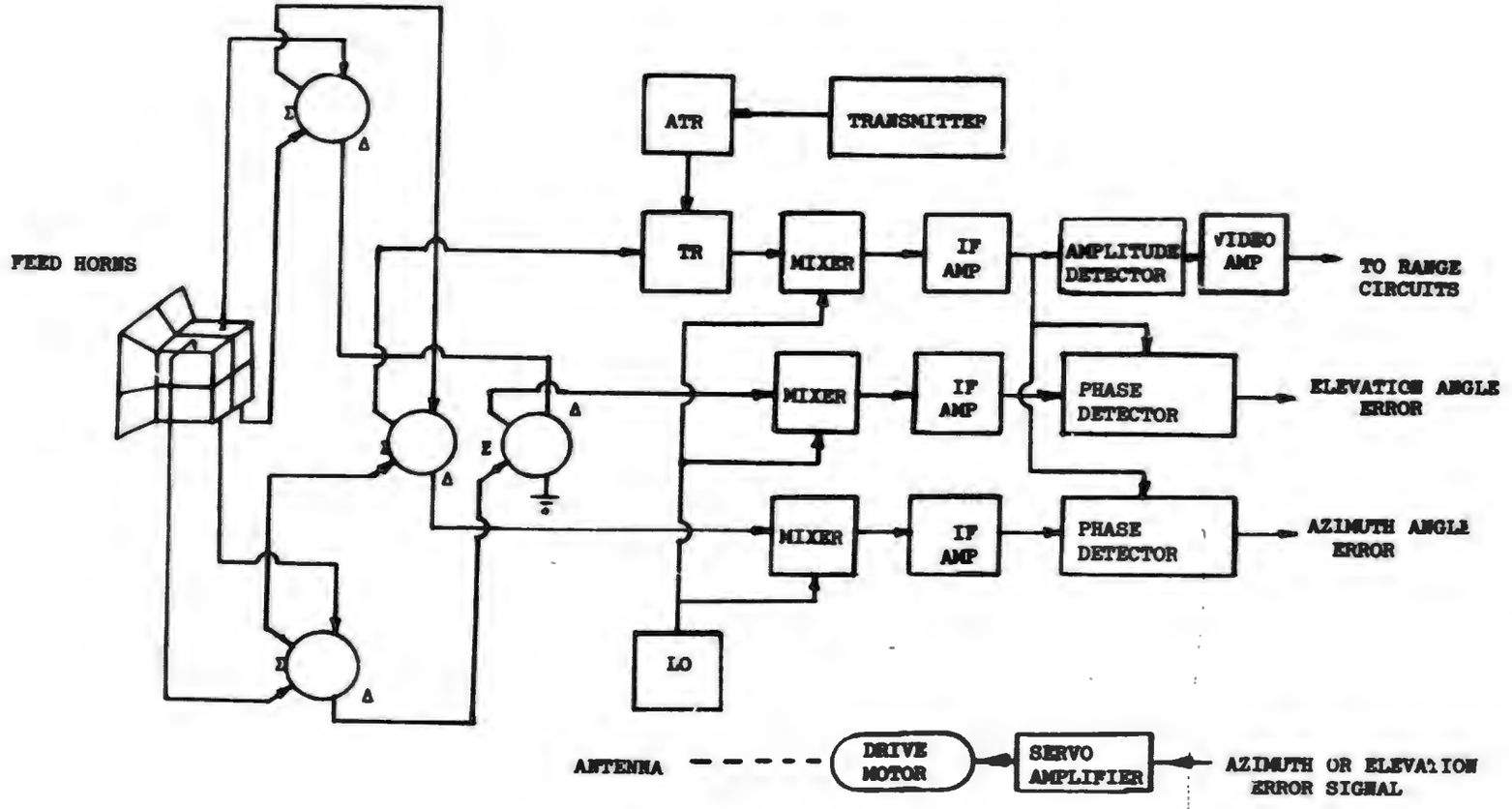

FIGURE 1 BLOCK DIAGRAM OF TWO COORDINATE (AZIMUTH AND ELEVATION) AMPLITUDE COMPARISON MONOPULSE SYSTEM

by passive hybrids before the signal reaches any active element. The four feeds generate the sum pattern, while the difference pattern is obtained by summing two adjacent feeds and subtracting the sum from the other two adjacent feeds. The difference pattern in the orthogonal plane is obtained by adding the differences of the orthogonal adjacent pairs. This system requires four hybrids to obtain the sum channel, the azimuth difference and elevation difference channels. The sum and difference channels are mixed to IF by means of a common oscillator, so that phase coherence is maintained between the channels. The signals are then amplified and the two difference signals applied to a phase detector to obtain angle error information that closes a servo system to position the antenna. The sum signal goes to an amplitude detector to obtain range information. These channels are the equivalent of three complete receivers that must be carefully gain- and phase- matched over the required dynamic signal range and bandwidth. Any lack of phase match between an error channel and the sum channel will result in a reduction in loop gain and a boresight error for that channel.

A block diagram of a mechanical track-while-scan radar with provisions for obtaining error signals is shown in Figure 2 (only a single angular coordinate is shown since both channels are identical). The electrical characteristics of the beam formed by Foster, Robinson or Lewis scanners are nearly identical, the major difference being in the mechanical construction of the beam forming scanner. Of these three, the Robinson Scanner has found the widest application by Army in its (AN/MPQ-4) Mortar locators; the Navy used the Foster Scanner for a shipboard (AN/SPS-8) height finding radar.

The Lewis Scanner Antenna is a lens antenna which produces a narrow fan shaped beam which is scanned in a linear, sawtooth motion through moderate angular range. It scans a sector by sweeping through the sector with constant angular velocity; then quickly returning to its starting point and repeating the scan. Although the scan is mechanically driven, high rates are achievable since the scan is generated by continuous rotary motion of a small feed horn.

A single channel mechanical TWS can be analyzed in the same manner as a conical scan tracking radar by considering the scan rate to be analogous to the mutation rate of the rotating feed. As in conical scanned trackers, the echo signal will be modulated at a frequency equal to the scan frequency of the beam. The amplitude of the echo signal will depend upon the shape of the antenna pattern and the squint angle. (The squint angle, as used here, is the angle between the major lobe axis on successive scans, rather than the angle between the axis of rotation and the axis of the antenna beam.) The scan modulation is extracted from the echo signal and applied to a servo control system to position angle gates and the antenna.

The same motor that drives the scanner can provide the reference signal, but there are usually three magnetic switches mounted in the scanner head which generate the start, center and stop pulses of the scan.

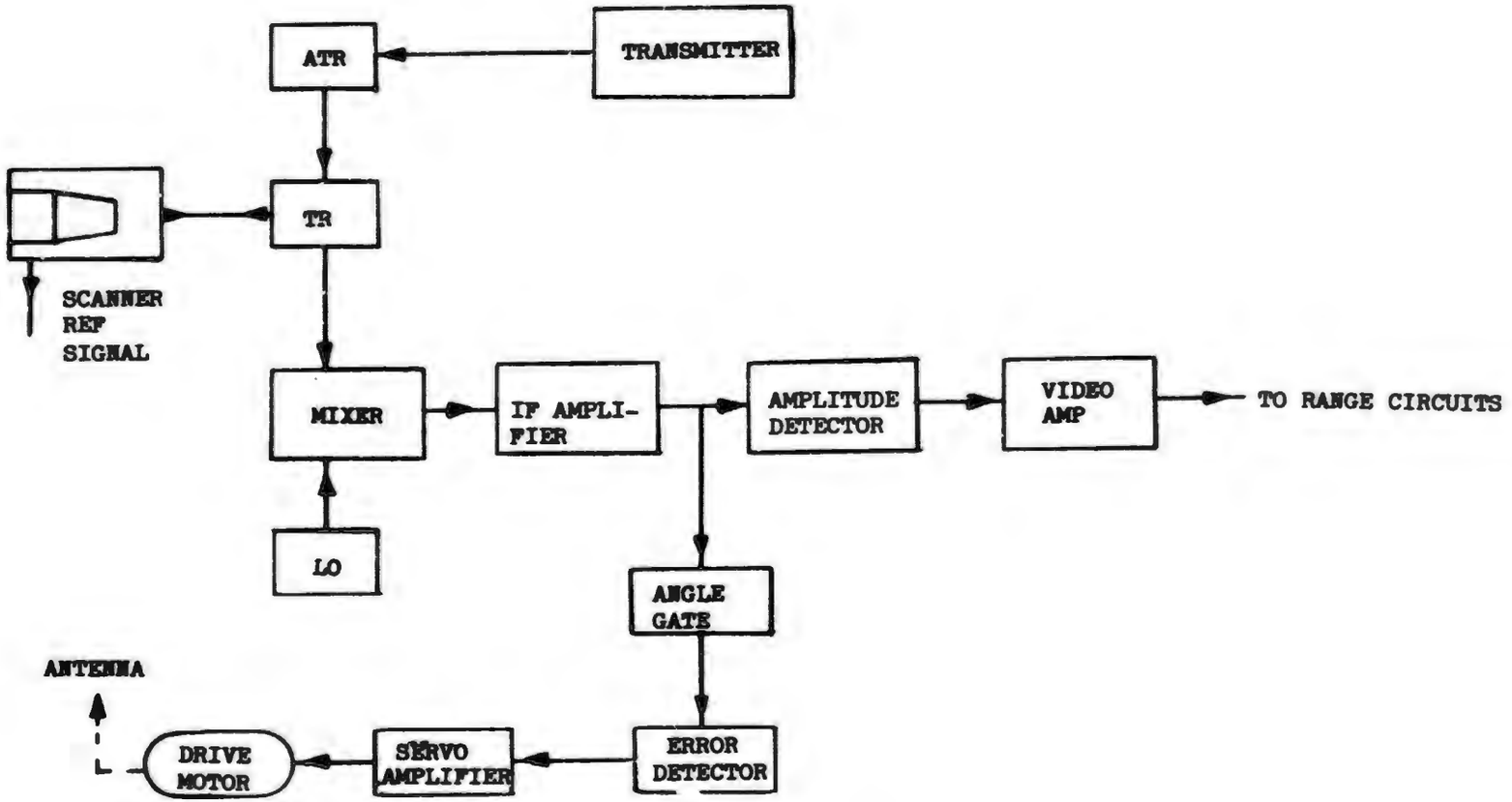

FIGURE 2 BLOCK DIAGRAM OF TRACK-WHILE-SCAN RADAR SYSTEM
(SIMPLIFIED ONE ANGULAR COORDINATE CHANNEL)

The receiver is a conventional superheterodyne except for two features peculiar to the TWS radar. One feature not found in other radar receivers is a means of extracting the angle error signal. This is accomplished after the second detector, in the video portion of the receiver, by using electronic angle tracking loops similar to those used for range tracking. The error signal output is used to position both the angle gate and drive the antenna servo motors. The angular position of the target may be determined from its position within the sector and/or from the antenna axis.

COMPARISON OF TWS AND MONOPULSE RADARS

A qualitative comparison of antenna construction shows that the monopulse system is a more complex assembly with a large amount of plumbing required for feeds, hybrid mixers, and RF lines running back to the transmitter. The antenna and feed designs for the TWS are electrically more simple, but introduce the mechanical problems of shaping the antenna and balancing the scanner feed. This has led to wide use of electronic scanning. Appendix I describes the design of the Lewis Scanner Antenna. Monopulse Antenna System Design information is available in the references.

RECEIVER AND DETECTORS

A simple IF amplifier with enough AGC to prevent overloading and a stretching or "boxcar" operation for angle and range tracking is all that is required for a single channel track-while-scan system as shown in Figure 2. In comparison, the monopulse receiver (Figure 1) must maintain both the gain and phase shift of all three channels. Any differences in gain or phase would be interpreted as erroneous angular errors. The range tracking in both systems uses the same simple boxcar technique that is used in most range trackers and will be discussed later.

ANGLE MEASUREMENT ERROR ANALYSIS

The angular accuracy of tracking radars is influenced by such factors as the mechanical properties of the antenna and pedestal the method by which the angular position is measured, the type of servo system, the stability of the electronic circuits and receiver noise figure.

Errors in tracking or measurement can be divided into two classes: systematic (or bias) and random (or noise). By choosing mathematical models which are close approximations of actual error components, we can obtain an accurate analysis of the error in the system by using both test data and theory and then extrapolating the results to many operating situations. These errors are summarized in Tables I and II.

The error in any given measurement can be defined as the difference between the value measured and the true value of the measured quantity.

Thus, the purpose of this error analysis was to provide a description of the error and to estimate the magnitude for all possible conditions.

The monopulse system (Figure 1) uses three identical gain controlled IF amplifiers: one each for reference, azimuth and elevation. The Automatic Gain Control (AGC) is derived from the range tracking loop and is proportional to the detected reference signal. The azimuth and elevation signals are compared with the reference signal in a phase comparator. The output of the phase comparator is a video signal whose amplitude is proportional to the error IF signal and whose polarity is a function of the IF phase difference between the reference and error signal. This signal is coupled to the servo amplifier loop which positions the antenna to null out the error.

The track-while-scan radar (Figure 2) employs automatic tracking loops to position the antenna. This is accomplished when operating in the track-while-scan mode by feeding the angle analog error voltage from the tracking loops into the antenna servo system.

Figure 3 is a functional block diagram of this over-all tracking loop. The tracking loop consists of operational amplifiers, quarter square dividers and a phantastron circuit and comparator with the angle data obtained by measuring the elapsed time between start and stop pulses of the scanner and the angle gates. That is, the angle start pulse is derived from the scanner start (live) time and angle stop time from the leading edge of the late angle gate. Since there is no synchronization between the scan frequency and the PRF, there is often a variation of $\pm$ one target hit within the angle gate. Thus, the bandwidth of the angle tracking system should be limited to a frequency that is capable of tracking high speed (MACH - 1 or 2) targets on a pass course at close range (within 5 NM of the radar). Since the antenna servo bandwidth will be greater than the tracking loop, the response of the angle tracking system will be limited by the angle tracking loop. Figure 4 shows a typical tracking loop bandwidth. Appendix II discusses the design of the tracking loops in detail.

In addition to their primary task of following the target, the tracking loop provides gates and triggers for the display system. Also time selected AGC pulses are derived within the tracking loop, thereby making it possible to track multiple targets through a common receiver. The number of targets to be tracked with the sector is limited only by the number of tracking loops used in the system, since each loop is independent of the other for a fixed azimuth/elevation sector.

TABLE I

SYSTEMATIC AND RANDOM ERRORS

COMPONENTS	BIAS	NOISE
Radar-dependent Tracking errors (deviation of antenna from target)	Boresight axis collimation Axis shift with: r-f and i-f tuning, receiver phase shift, target amplitude, temperature; Wind Force; Antenna unbalance; Servo unbalance	Receiver thermal noise; Multipath (elevation only); Wind Gusts; Servo electrical noise; Servo mechanical noise
Radar-dependent translation errors (error in converting antenna position to angular coordinates)	Leveling of pedestal; North alignment; Static flexure of pedestal and antenna; Orthogonality of axis; Solar heating	Dynamic deflection of pedestal and antenna; Bearing wobble; Data gear nonlinearity and backlash; Data take-off; nonlinearity and granularity
Target-dependent tracking errors	Dynamic lag	Glint; Dynamic lag variation; Scintillation; Beacon modulation
Propagation errors	Average refraction of troposphere; Average refraction of ionosphere	Irregularities in tropospheric refraction; Irregularities in ionospheric refraction
Apparent or instrumentation errors (for optical reference)	Telescope or reference instrument stability; Film emulsion and base stability; Optical parallax	Telescope, camera or reference instrument vibration; Film transport jitter; Reading error; Granularity error; Variation in optical parallax

TABLE II

Summary of Tracking Error Equations:

1. Thermal Noise $\sigma_t = \dfrac{\theta}{\sqrt{\dfrac{2S}{N}\dfrac{f_r}{B_n}}}$ radians (for S/N > 1)

2. Multipath $\sigma_m = \dfrac{\theta_p}{\sqrt{8A_s}}$ radians

3. Target Glint $\sigma_g = 1/4 \dfrac{L_t}{R}$ radians

4. Servo Lag $\varepsilon = \dfrac{W_t}{K_v} + \dfrac{\dot{W}_t}{K_a}$ radians

5. Propagation Noise $\sigma_p = 2\Delta N \times 10^{-6} \sqrt{L/L_o}$ radians

SYMBOLS:

θ = radar beamwidth (radians)
S/N = Signal-to-Noise power ratio
f_r = repetition rate (pps)
B_n = servo bandwidth (cps)
p = ground reflectivity (voltage ratio)
A_s = Sidelobe attenuation power ratio
L_t = Span of target*
*(any consistent units)
R = Range of Target
W_t = Target angle velocity (radians/sec)
K_v = Velocity error constant (1/sec)
K_a = Acceleration error constant $\approx 2.5B_n$ 2 ($1/sec^2$)
ΔN = RMS variation in tropospheric refractivity (n-Units, or [n-1] x 6^{+6})
L = Length of tropospheric anomalies*
*(any consistent units)
L_o = Scale length of anomalies
σ = Noise NOTE: Subscript added to differentiate between different types of noise.

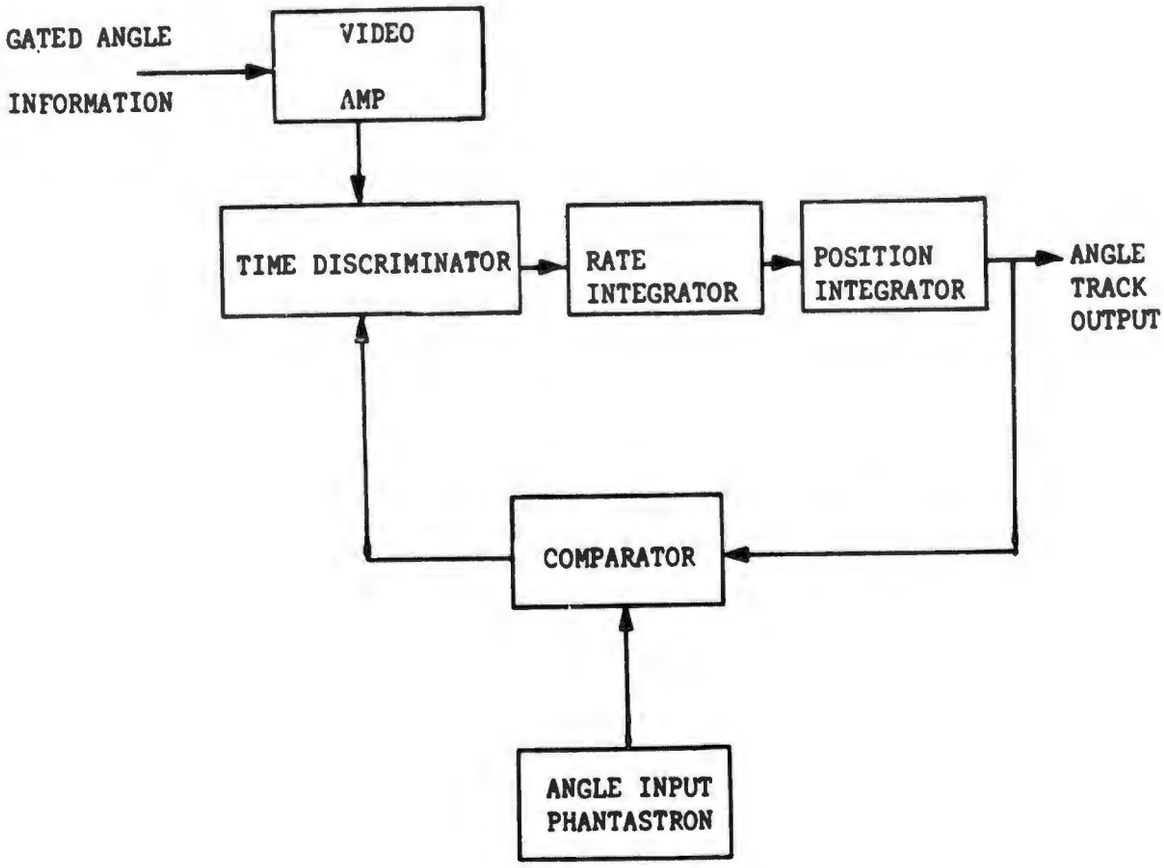

FIGURE 3. FUNCTIONAL DIAGRAM OF ANGLE TRACKING LOOP

RANGE MEASUREMENT ERROR ANALYSIS

Both TWS and monopulse radar use "simultaneous gating" techniques for automatic range tracking. This technique is based on the split gate (early-late gate) similar to the previously discussed angle gate; to reiterate, two range gates are generated as shown in Figure 5. One is the early gate and the other is the late gate. The echo pulse is shown in Figure 5 (a), the relative position of the gate at any particular instant in Figure 5 (b) and the error signal in Figure 5 (c).

The magnitude of the error signal is a measure of the difference between the center of the pulse and center of the gates, and the sign determines the direction the gates must be repositioned by the servo system to reduce the error signal to zero and to position the gates so they are centered on the target.

LOOP	BANDWIDTH POSITION	ω_3	ω_5	ω_4
ANGLE	1	.1	.14	.2
ANGLE	2	.4	.56	.8
ANGLE	3	1.0	1.4	2.0
RANGE	1	.4	.56	.8
RANGE	2	1.0	1.4	2.0
RANGE	3	4.0	5.6	8.0

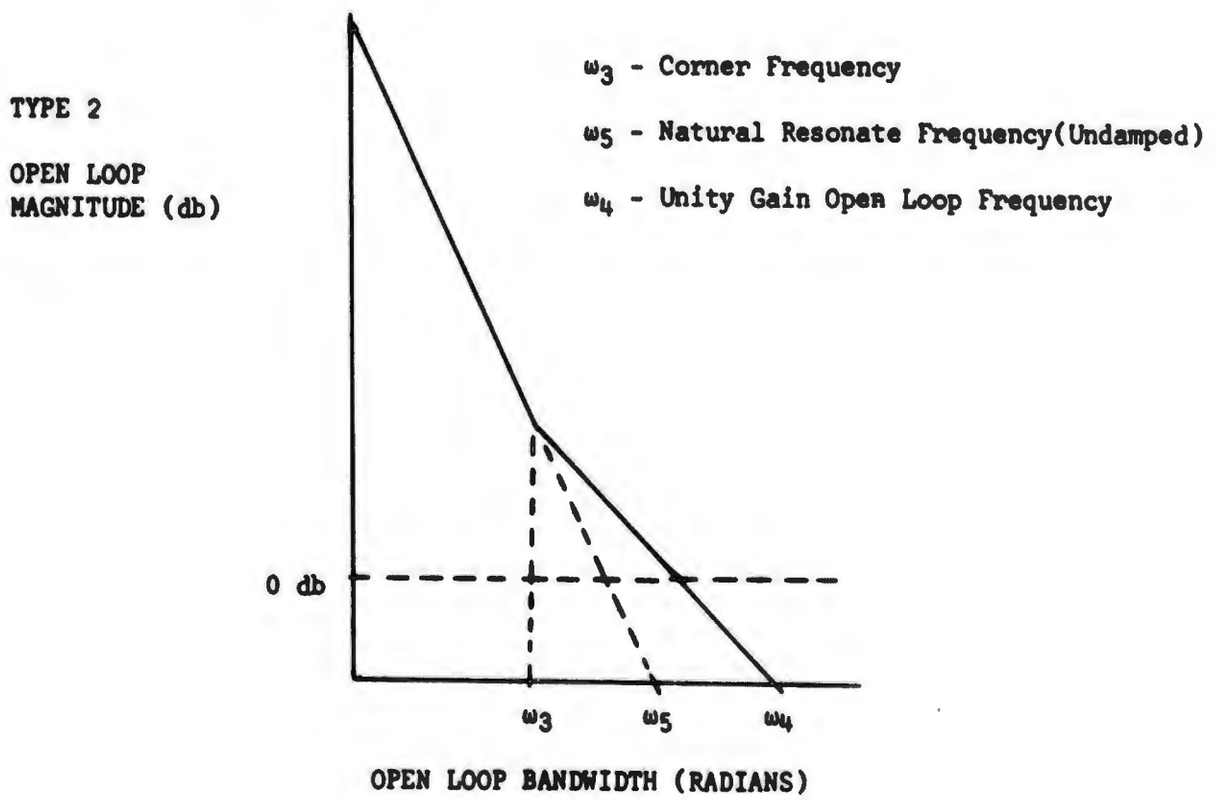

FIGURE 4 - TRACKING LOOP BANDWIDTH

(a) Echo Pulse:

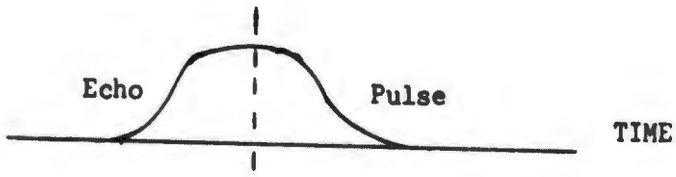

(b) Early-Late Gate:

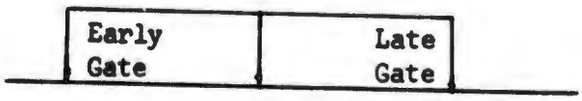

(c) Difference Signal Between Early and Late Gates:

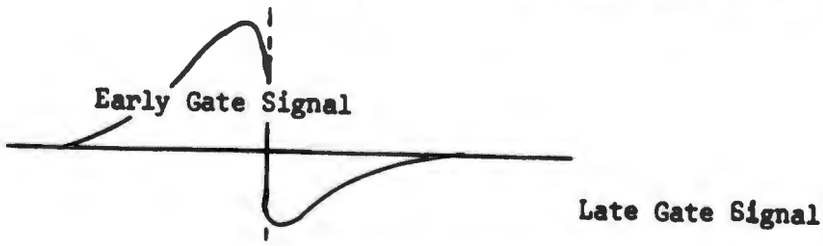

FIGURE 5 - SPLIT RANGE GATE TRACKING

Range gating, just like angle gating, is necessary to perform automatic tracking and has several advantages as byproducts; i.e., it isolates the target of interest, excluding targets at all other ranges, thus permitting a boxcar generator to be employed and improves signal-to-noise ratio since it eliminates the noise at other ranges.

As in the analysis of the angle tracking, the system errors which are encountered have been well defined and are summarized in Table III.

These range error components are fixed in rms value, and may be evaluated periodically or at the time of normal maintenance testing. Typical values for fixed components of both bias and noise are in the order of 7 feet, rms. In addition, variable noise components are as follows:

Thermal noise error $\sigma_{rt} = \dfrac{\tau}{\frac{S}{N}\frac{f_r}{B_n}}$

Multipath error $\sigma_{rm} = \dfrac{ph \sin E}{8A_s}$

Target glint $\sigma_{rg} = 1/4\ L_t$

Servo lag $\Sigma_r = \dfrac{V_t}{K_v} + \dfrac{A_t}{K_a}$

Propagation noise $\sigma_{ra} = \Delta N \times 10^{-6}\ 2L_oL$

In the above, τ is the pulse width expressed in equivalent radar range (1μsec = 500 ft); h is the antenna height; E the target elevation; V_t the target velocity; A_t the target acceleration; and the other symbols are as used earlier.

TABLE III - INVENTORY OF RANGE ERROR COMPONENTS

COMPONENT		
Radar-Dependent Tracking Errors	Zero Range Setting Range Discriminator Shift Servo Unbalance Receiver Delay	Receiver Thermal Noise Multipath Servo Electrical Noise Servo Mechanical Noise Variation in Receiver Delay
Radar-Dependent Translation Errors	Range Oscillator Frequency Data Take-Off Zero Setting	Range Resolver Error Internal Jitter Data Gear Nonlinearity and Backlash Data Take-Off Nonlinearity and Granularity Range Oscillator Instability
Target-Dependent Tracking Errors	Dynamic Lag Beacon Delay	Dynamic Lag Glint; Scintillation; Beacon Jitter
Propagation Error	Average Tropospheric Refraction Average Ionospheric Refraction	Irregularities in tropospheric refraction Irregularities in ionospheric refraction

TRACK-WHILE-SCAN RADAR ACCURACY EVALUATION

The following evaluations are concerned with the radar accuracy and tracking performance under field conditions after installation of the radar. The results of these evaluations are intended to identify TWS system capabilities.

The accuracy determinations are based on comparisons between radar measurements (azimuth, elevation and range) and translated data from a reference system. (In this case, the AN/FPS-16 system furnished the reference data.)

The tests were conducted in two phases: first, on the TWS radar, using its on-site real-time data monitoring equipment and range azimuth scopes; second, using the electronic data system, which included an IBM 7094 computer for data processing. In both cases, the AN/FPS-16 was the referenced radar.

The initial tests were conducted on the radar to determine the angle accuracy and range accuracy including errors between the tracking loops using both static bore site testing and an aircraft with beacon test flights so that a comparison between tracking loops could be made by simultaneously comparing skin and beacon tracks.

These tests indicated that the radar after installation and checkout had the following accuracy:

Azimuth	- 0.8 mil
Elevation	- 0.8 mil
Range	- 6 yards

After the Electronic Data System was installed and checked out, additional testing was conducted on the system, again using the AN/FPS-16 radar reference. These tests evaluated the data system interfaced to the IBM 7094 computer and consisted of a number of orbital, radial and tangential flights. Although the radar originally had met the one-mil accuracy requirements after installation, the data now indicated that there was a 1.5 mil angle error in the system which now included the data takeoffs and 7094 computer.

Analysis of the track data indicated that there was a rapid azimuth perturbation as if the radar antenna were oscillating or hunting around the target. Further analysis of the antenna positioning system indicated that the servo system and digital encoders were introducing errors in the data. The existing servo system did not use an intermediate servo amplifier and the azimuth digital encoder shaft had developed excessive backlash. A detailed analysis of the servo system revealed that the tachometer feedback signal contained high frequency acceleration components causing the servo to overshoot in both the clockwise and counterclockwise directions. To correct this problem, an electronic intermediate servo amplifier with zero velocity lag was installed, including a filter, to reduce the high frequency servo

response. The addition of the zero velocity lag intermediate servo system appeared to have reduced the angular acceleration of the antenna and drive motor so that the antenna servo system noise became a minor source of the overall tracking noise and completely eliminated the hunting. Therefore, no attempt was made to determine the source and magnitude of each source of the antenna servo system noise. The intermediate servo was designed so that the Tachometer error causes little servo system noise.

The stiffening of the expansion bellows reduced the backlash error in the encoder shaft to less than 0.1 mil. The encoder backlash is caused by bearing and slipping friction that causes a torsional structural flexure of the antenna encoder support.

Thus, using the intermediate servo to rotate the antenna and an optical technique to check flexure, the antenna can be rotated smoothly enough so that a seventeen bit encoder increases (decreases) its count at one bit (0.0026°) per second. This indicates that the encoder backlash causes a bias error and not a noise error in the data; (i.e., the friction which causes the encoder backlash has much higher sliding and viscous components than static components). If the encoder backlash were constant, the computer could correct the error because the intermediate servo turns the antenna so smoothly that the antenna is almost always turning slowly in one direction while tracking a single moving target and any non-correctable error would occur only during the brief time the antenna is reversing direction. To prevent backlash error changes from creeping into the system, a preventive maintenance procedure was established so that day-to-day checks between real-time analog plotting system and the optical system could be used to measure the encoder backlash.

Although the main purpose of these tests was to reduce the angle errors, the range tracking accuracy was rechecked after a high pass filter was added in the video line to improve angle tracking accuracy. This recheck indicated that there was no significant change in range tracking noise.

The error between two range tracking loops which are tracking the same video signal consistently had a standard deviation of less than four yards and a variation of the mean values of $\pm$ 2 yards. The maximum range of the mean value was less than $\pm$ 10 yards. Of this ten-yard variation, a repeatable bias error of minus four yards occurred when the target azimuth was about 20 degrees. This bias error diminished at other azimuths and became a plus 4 yards at about 200 degrees. This implies a 4-yard error in parallax correction, or most likely, the aircraft had to change its roll angle to compensate for the drift caused by the wind, which caused a change in the center of the target's radar cross section. Both static and flight tests were conducted to determine the system accuracy after the changes to the antenna servo system and data encoders were permanently installed. The results are listed in Table IV.

This analysis proved valuable for dual reasons; it demonstrates the basic radars performance and sheds light on the error contributing factors which are typical of field operations but are less likely to occur in the course of controlled system tests.

TABLE IV

TRACK-WHILE-SCAN ANGLE/RANGE ERRORS

SOURCE OF ERROR	*MAGNITUDE	
	AZ	EL
1. Tracking Loop Circuit Noise	.025	.025
2. Antenna Servo Noise	.20	.04
3. Tracking Error (Tangential Flight)		
a. Minimum	0.1	0.1
b. Normal	0.3	0.3
c. Maximum	0.7	0.8
4. Tracking Error (Radial Flight)		
a. Minimum	.2	.3
b. Normal	.4	.5
c. Maximum	.8	.7
5. Error between two tracking loops	0.15	0.4
6. Range		
a. Minimum	4	4.5
b. Normal	7.0	7.25
c. Maximum	10	10

*(ANGLE, MILS, RANGE, YARDS)

SUMMARY OF ERRORS

The contributions of the factors affecting the tracking error are summarized in Figure 6. The gross effects of each factor are shown. Curve A

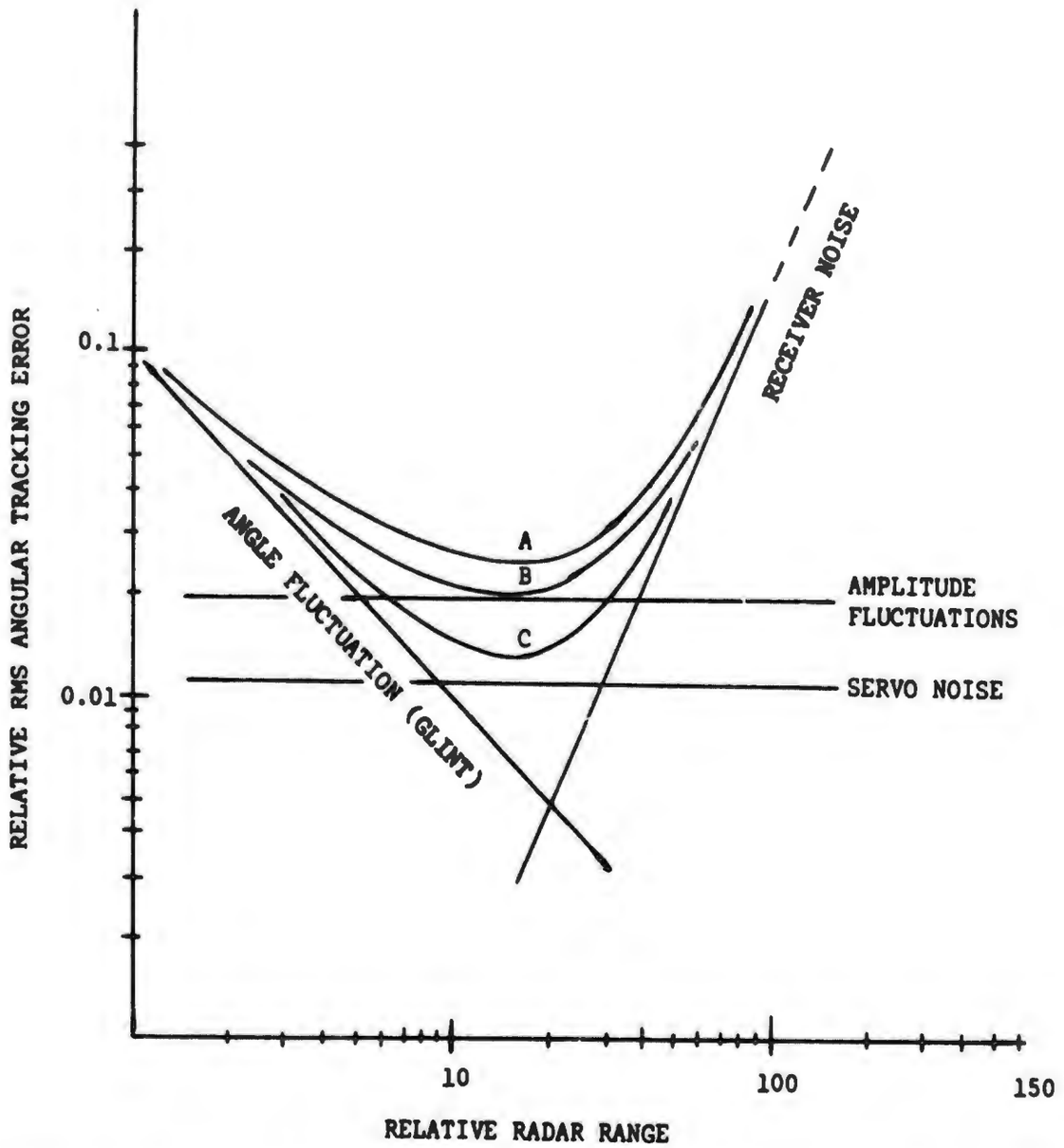

FIGURE 6 - Relative Contributions to Angular Tracking Error Due to Amplitude Fluctuations, Angle Fluctuations, Receiver Noise, and Servo Noise of function of range (A) Composite Error for Conical Scan (B) for Track-While-Scan (C) for Monopulse

is the sum of all effects, is representative of conical scan radars, and is shown for comparison only. Curve B contains less amplitude fluctuations and is representative of the TWS radars. Scintillation noise is usually lower than in conical scan, is higher than monopulse, and lies somewhere between the two. Curve C does not include the amplitude fluctuations and is representative of monopulse radars.

Since the TWS radars are similar to conical scan-radars [in that the tracking error is superimposed on a subcarrier at the scan frequency], the noise bandwidth is nearly twice that of the monopulse tracker having the same servo bandwidth and is sensitive to whatever scintillation component exists at the scan rate.

Major characteristics of the various types of tracking radars are tabulated in Table V. Included for comparison purposes is a conical scan AN/MPQ-12 which is a modified version of the SCR-584 radar.

A theoretical analysis of tracking errors for monopulse radars can be found in the publications of Rhodes, Barton, Berkowitz, Skolnik etc., and therefore, will not be covered here.

A theoretical analysis of the angle tracking loop errors for TWS radars is contained in Appendix III.

TWS tracking system errors caused by antenna nonlinearity are functions of the received signal frequency, the bearing of the target with respect to lens structure, and PRF of the transmitter.

Accuracy of angle loops - The change in antenna gain as the beam moves past the target amplitude modulates the received signal. If the antenna or scanner system is not linear, the change in signal strength will appear as noise in the servo system. This is true for both gradual and abrupt non-linearities and increases as fewer points are sampled on the antenna pattern during low PRF or scan rate operation.

The characteristic of this tracking noise is not random, but is related to the drift rate of the sampling relative to the target position in the scanned sector and response time of the angle tracking system. Noise due to changes in scanner speed causes a larger error for a target at the end of a scan than near the beginning of a scan since the bandwidth cannot correct for the speed changes.

The noise in angle measurement can be contributed to changes in scanner speed, antenna pattern sampling at low PRF rate, feed back signal and the tracking loop itself.

Some tracking noise is caused by the sampling and "box carring." The antenna beam is sampled at the PRF rates and shape must be sampled at least four times in order that the angle tracking circuits can measure the apparent center of the antenna pattern and determine the actual center by 1/2 the angle

of the beam during one PRF period. Errors which occur depend upon location of the sample compared to the center of the pattern.

Some noise in the angle tracking circuit is caused by the technique used to generate the variable time delay but is self correcting after one rise time of the tracking circuits.

The antenna servo system noise adds to the angle tracking noise because motion of the antenna is not fully cancelled by the feed back. In addition, any scanner nonlinearity will add to this error and increase servo noise.

COMPARISON/SUMMARY OF CHARACTERISTICS

There is little significant difference between the detection capability of mechanical TWS and monopulse trackers when the major parameters of the radar used in the radar equation are the same. Use of monopulse techniques results in slight loss in antenna gain over a non-tracking or scanning antenna of the same size because of the offset beams used for tracking.

The tracking accuracy of the TWS radar is degraded if the target cross section (signal) fluctuates in amplitude at frequencies at or near the scan frequency, whereas amplitude fluctuations have essentially no effect on the monopulse radar. The monopulse radar is the more complex of the two because of separate receivers required to derive the error signals. However, the TWS presents mechanical problems in fabricating the antenna.

With the monopulse tracker, it is possible to obtain a measure of the angular error in two coordinates on the basis of a single pulse; a minimum of a single scan containing at least four pulses is required for the TWS radar. Thus, TWS radar scan rate is limited by the PRF and by the requirement of receiving at least four (4) pulses in any one scan cycle to obtain target error information.

The monopulse radar is capable of tracking only a single target at a time in its tracking sector. If one chooses to track other targets, you must drop the present track and go through the procedure of search, acquire, and lock-on every time you track a new target within the sector of interest. On the other hand, the TWS can simultaneously track as many targets in sector scanned as there are sets of tracking loops and the problem of search and target acquisition is greatly reduced.

This characteristic makes it very desirable for use as a Ground Control Approach radar and where there are parallel runways in operation, one equipment can handle both runways simultaneously.

In summary, the performances of the TWS and monopulse radars are quite comparable, with two notable exceptions. When the amplitude of the target cross section fluctuates at a rate near the scan frequency, the TWS performance is degraded. When multiple targets must be tracked simultaneously, a TWS system must be used because the monopulse radar can track only one target at a time.

TABLE V

COMPARISON OF TRACKING RADAR CHARACTERISTICS

CHARACTERISTIC	AN/MPQ-12	AN/FPS-16	TRACK-WHILE-SCAN
Type of Tracking	Conical Scan	Monopulse	TWS Rolled Reflector Scanner
Antenna Size Ft.	10 Dish	12 Dish	17
Frequency	S Band	C Band	S Band
Beam Width Deg.	2.4	1.2	1.5
Pulse Width	0.25 μsec	0.25, 0.5, 1.0 μsec	.5, 1.0 μsec
Receiver Noise Figure	12	11	12
Receiver Bandwidth MHz	--	8.0 or 1.6	12
Accuracy:			
Range	10 yards	5 yards	8 yards
Angle	1 Mil	0.1 Mil	0.5 Mil

APPENDIX I

LEWIS SCANNER DESIGN

1.0 Background on Lewis Scanner (US Patent No. 2,585,562)

This scanner, which was first described by Lewis of Bell Telephone Laboratories at the First Scanning Symposium held at MIT in 1943, provides a very convenient technique for rapid feed motion. Initial data presented showed side-lobe levels of the order of 12 db over the scan angle. These lobes were highest at the scan limits. It was impossible to obtain dead time less than 20 percent.

In the Third Scanning Symposium, W. C. Wilkinson of RCA Laboratories described a K-Band Lewis Scanner. This equipment was electroformed to provide smooth parallel plate surfaces. No data was presented on the gain which was measured, but it was indicated that some difficulty was encountered in this area; Wilkinson indicated a loss in gain of less than 4 db when questioned on this matter at a later date. The lens utilized was a dielectric structure and it was necessary to employ absorbing cloth between the lens and the parallel plate conductor. This undoubtedly was the cause of some loss in gain.

In the Fourth Scanning Symposium, discussion of the AN/TPQ-2 Lewis Scanner at Georgia Institute of Technology indicated losses in the parallel plate region of the order of 4 db. This, too, utilized dielectric lenses in which difficulty was encountered in contact with the surfaces of the parallel plates. In this model, some trouble was encountered with warpage and, hence, defocusing. Cracks and surface roughness contributed strongly to the losses. At the Fourth Scanning Symposium, Budenbom indicated that a 4-db loss in gain had been measured on a similar unit at Bell Telephone Laboratories, but it appears that the program was terminated before final design had been accomplished.

Based upon past history, it is evident that for optimum gain performance, the dielectric lens should be eliminated; the parallel plate structure should be maintained as smooth as possible; and the over-all antenna supports should be of sufficient and massive construction to maintain mechanical tolerance under the temperatures and other environmental conditions.

2.0 Theory of Lewis Scanner

2.1 Objectives

The Lewis Scanner is a device for producing a beam of RF energy which may be swept linearly in one direction. Movement of the beam is controlled by rotating a relatively small feed, the major portion of the structure remaining motionless.

2.2 Optical Considerations

Figure 1 (a) shows the plan view of a parallel plate structure with a

lens at the wide, or output end. This is a bifocal lens which has foci at the points C and D. The focal path is approximated by an arc containing C and D, with its center at the center of the lens. If a source of RF energy is located at D, the ray diagram is as shown in Figure 1 (a). The path lengths of all rays from D to the line U_1 U_2 T_3 are equal; hence the line U_1 U_2 T_3 represents the phase front. The axis of the main beam will be perpendicular to this phase front. The angular deviation of this beam from the centerline of the structure is 0, which is equal to the angle between the central ray DS2 and the centerline. This relationship is exactly true only for energy sources located at the foci C and D, but is very nearly true for a source at any point P along the focal arc. The beam may be caused to swing from left to right by moving the energy source from C to D. The two-dimensional geometry in Figure 2 shows the general optics of the antenna.

2.3 Physical Considerations

In the configuration described, it would be mechanically cumbersome to move a source of radio energy along the focal path to produce rapid, linear, one-way scanning of the beam. The unit must be modified to make such beam motion practicable.

Consider a plane reflector EF introduced in the system, as shown in Figure 1 (b). It is seen that the focal arc CD is reflected as the arc C'D' becomes the circular base of the cone. This configuration is shown in Figure 1 (d). The source of radio-frequency energy may now be made to traverse this circle, and the beam will swing from say, the right side of the lens to the left side, then reappear at the right and repeat its scan. The scanning motion is linear with source rotation and since the source may be a relatively light-weight horn, very high scanning rates may be obtained. The mechanical configuration shown in Figure 3 is the result of forming large parallel plate waveguide into a cone. The feed end of the antenna is the large cone on the underside of the two perspective views. The scanner fly wheel contains a curved feed horn which directs the energy into an angular opening at the base of the cone. Microwave energy is channeled through the cone and collimated by the lens to form a beam which is narrow in the plane that is focused by the lens and finally radiated by the aperture horn.

3.0 Lens Design

A fundamental problem in the Lewis technique is in the design of the collimating lens mentioned previously. Two general types may be used; either the dielectric lens or the metal plate lens. The dielectric lens is inherently broad band, but has severe power handling (and to a lesser extent, efficiency) limitations. Of lesser importance in the system under discussion is its weight. A preliminary study of dielectric lens techniques showed that this approach was inappropriate primarily because of efficiency considerations. It was also recognized that severe power handling problems were likely if this course were chosen.

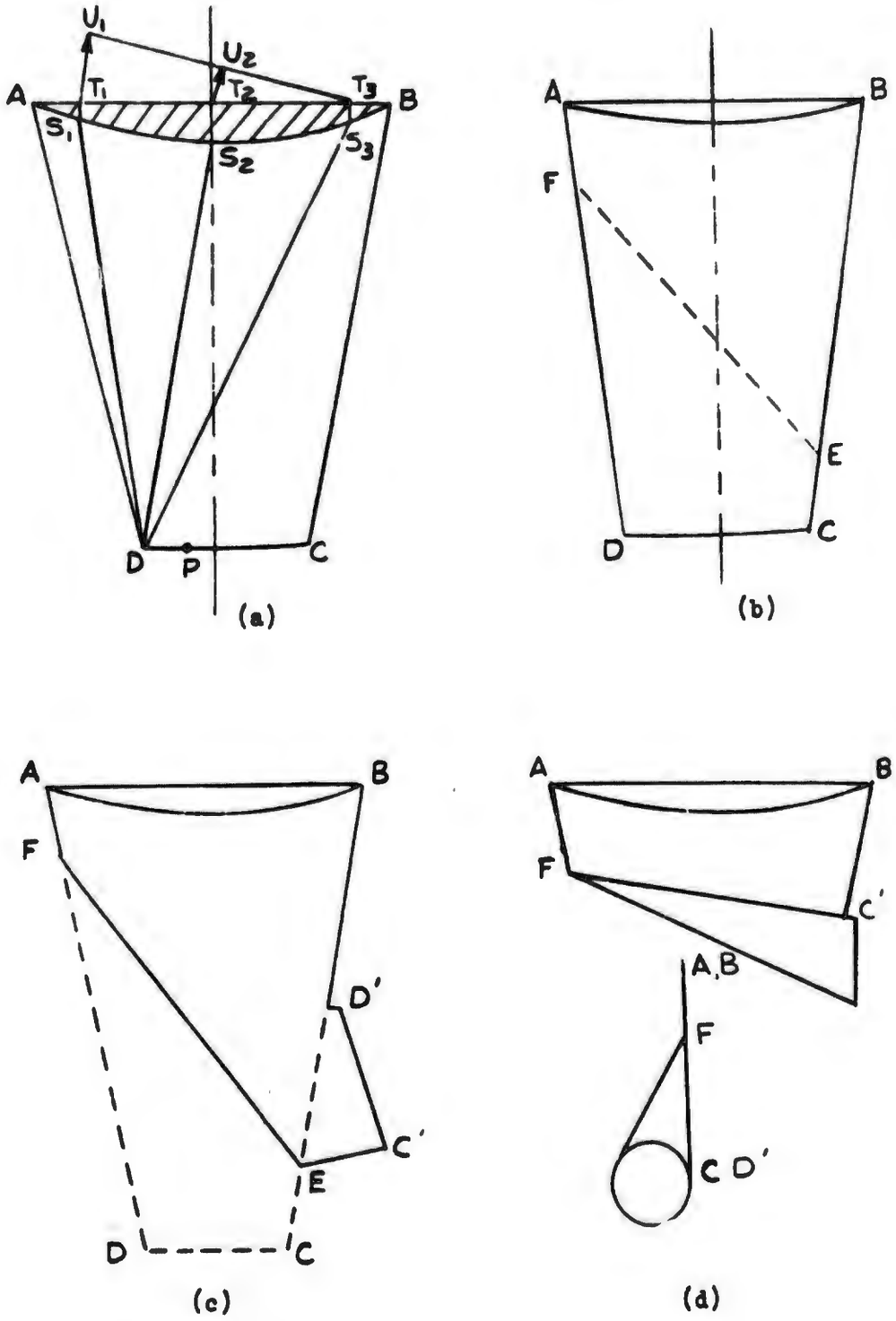

FIGURE 1 LEWIS SCANNER, OPTICAL AND PHYSICAL CONSIDERATIONS

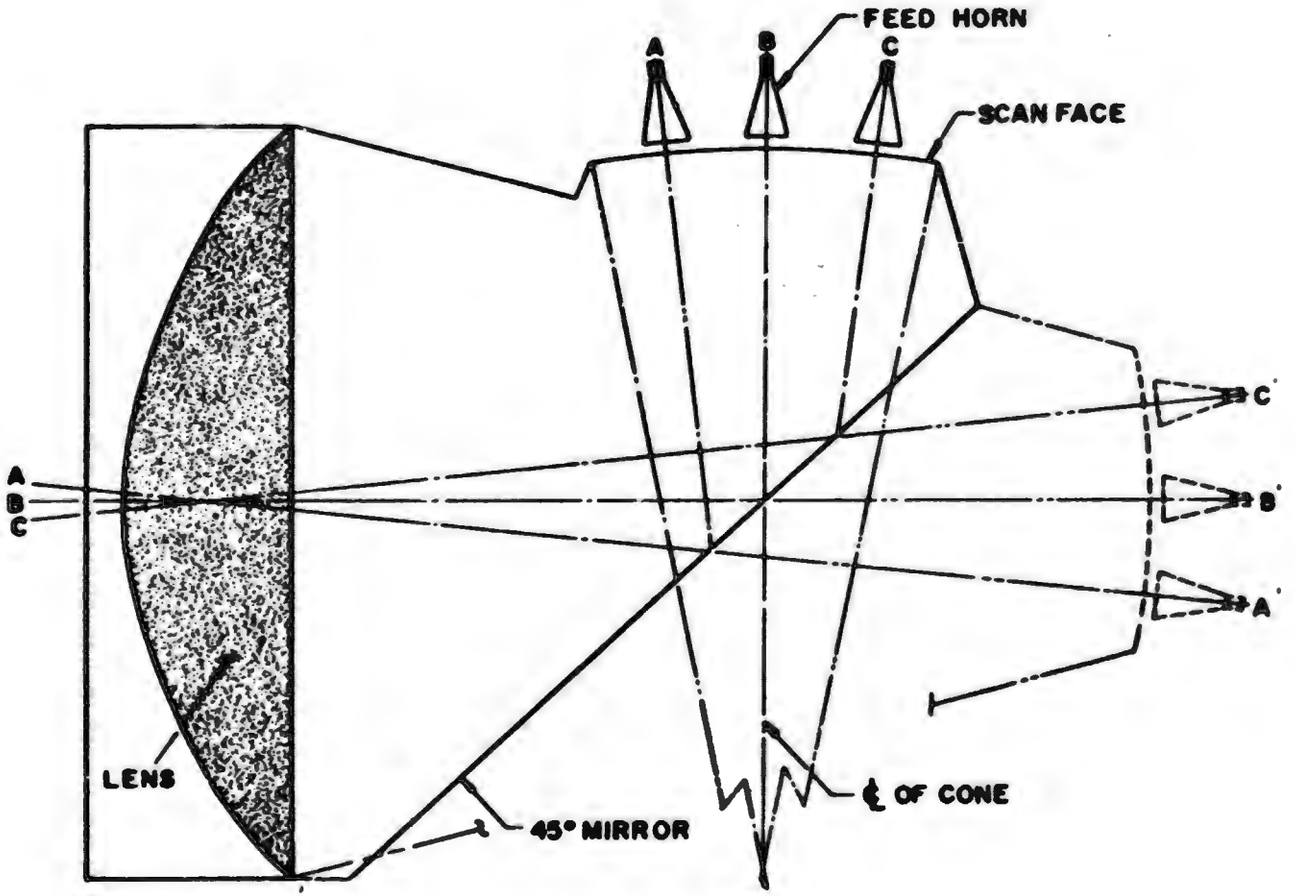

FIGURE 2 LEWIS SCANNER ANTENNA GEOMETRY

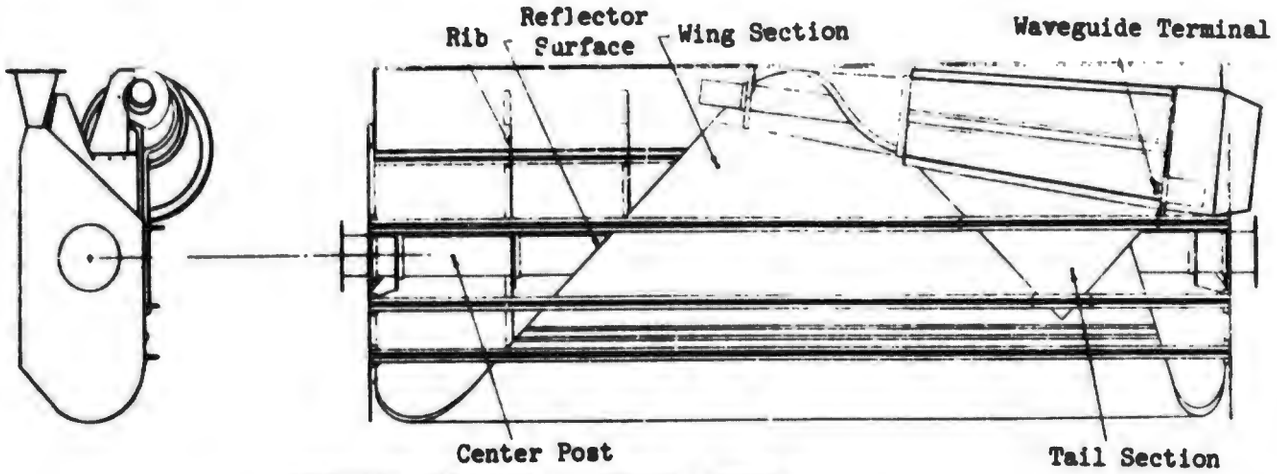

ORTHOGRAPHIC VIEW OF ANTENNA BOTTOM

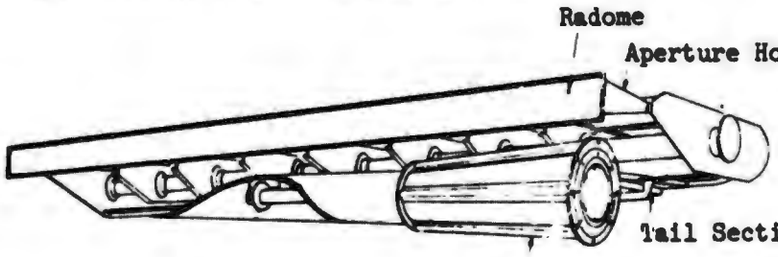

VIEW LOOKING INTO FRONT OF ANTENNA

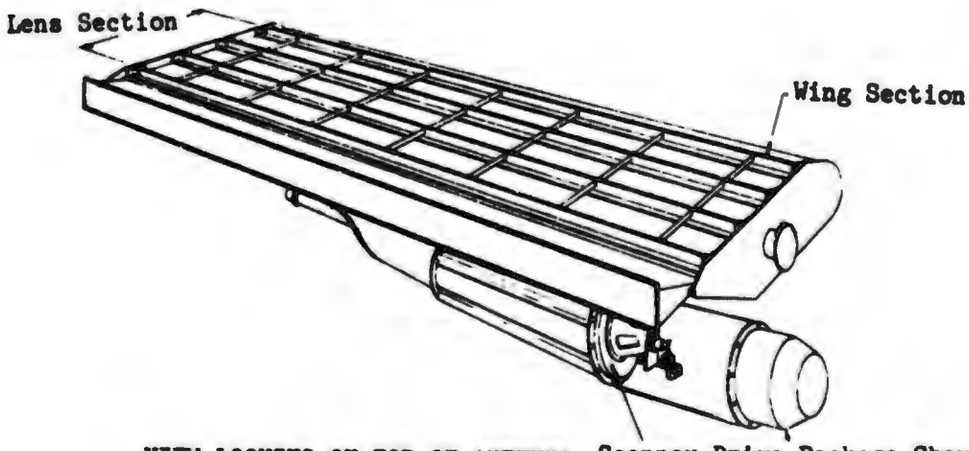

VIEW LOOKING ON TOP OF ANTENNA

FIGURE 3 LEWIS SCANNER ANTENNA CONFIGURATION

The metal plate lens is light in weight, relatively economical to fabricate and provides high efficiency and power handling ability. All of the many versions make use of a number of waveguide sections whose dimensions and consequently velocity of propagation are chosen to provide the desired focusing action. Since the velocity of propagation is a function of frequency as well as dimension, the metal plate lens is a relatively narrow band device. Choice of the constrained lens type was a compromise decision in which efficiency and power handling were obtained at the sacrifice of bandwidth.

4.0 Feed System Design

For best performance, illumination of the lens should be tapered quite sharply requiring a fairly large feed horn aperture; dead time, however, is limited to 20 percent of the scan cycle. The feed horn, therefore, must have a smaller-than-optimum aperture to assure its being entirely clear of the dead zone during 80 percent of the scan cycle. Increasing the ratio of focal length to lens width improves the lens illumination but limits the total scan angle. As the horn aperture is decreased, the lens is illuminated and the sidelobe level is increased. The feed horn pattern or shape can be controlled by obstructing the horn aperture, however, this results in low power-handling capabilities and poor impedance matching. It should be noted that no design combinations of focal length or scan angle will eliminate the dead time problem.

5.0 Scanner Assembly

The RF pulse energy from the transmitter enters the scanner head section of the antenna via a high speed rotary joint. The latter is waveguide coupled to a rotating horn which injects the RF into the slot between the rolled parallel plates leading to the output horn.

Fabrication of the scanner feed was probably the most difficult task of the whole system. Problems, such as high speed drive, balancing and waveguide matching, were encountered.

Essentially, the scanner feed parts are aluminum castings which have been machined after casting. Stainless steel inserts are pressed into the castings where bearing surfaces are required. In order to minimize dynamic balancing problems at high speeds, it is essential that all parts be concentric.

The feed horn was machined from aluminum stock and dipbrazed. Pressure-sealing this unit was a major problem. A 0.010 inch thick mylar window had to be mounted on the output flare of the horn; this was the source of the sealing problem. The window was finally sealed to the horn using epoxy adhesive and aluminum bezel which was fastened to the horn using flush head machine screws.

The complete scanner disc assembly, excluding the rotary joints, was dynamically balanced on an automative crankshaft type machine. This was found to be suitable for initial balancing; however, we found that at first, balancing had to be performed on the machine used for balancing aircraft turbine engine motor assemblies. The balancing was accomplished by removing material and adding weights. Because of the high speed operation and balancing problems, the machining tolerances of all pieces on the scanner feed assembly were quite critical.

APPENDIX II

TRACKING LOOP DESIGN

1.0 Tracking Loop Design

Figure 1 can be used to analyze either the range or angle tracking loop provided the video block is interpreted properly. In the case of range, the video consists of the discrete pulses returned from the target that fall within the angle gate. In the case of angle, the video is the boxcar which is composed of the stretched and dumped pulses within the angle gate. The angle video, therefore, looks like the antenna pattern, provided a linear receiving system is used. Although the tracking loops are sampled-data control systems, they can be approximated by continuous control systems when the sampling frequency is much higher than the corner frequency (ω_o).

2.0 Transfer Function

From Figure 1, the transfer function of the tracking loop is

$$\frac{T_o(S)}{T_i(S)} = \frac{K_c K_d G(S)}{1+K_c K_d(S)} \qquad (1)$$

where

T_i is the input video pulse,
T_o is the split tracking gate,
K_c is in Sec/Volt (Comparator gain),
K_d is in Volts/Sec (Discriminator gain),
G(S), the product of the two integrator transfer functions, is:

$$G(S) = \frac{r}{R_1 R_2 C_2} \quad \frac{S+1/C_1}{S^2} \qquad (2)$$

Resistor (r) provides the phase lead that is necessary for loop stability.

The gain factor is

$$K = \frac{K_c K_d\ r^2\ C1}{R_1 R_2 C_2} = \frac{\omega_4}{\omega_3} = 2 \qquad (3)$$

and the corner frequency is

$$\omega_o = \frac{1}{r\ C_1} \qquad (4)$$

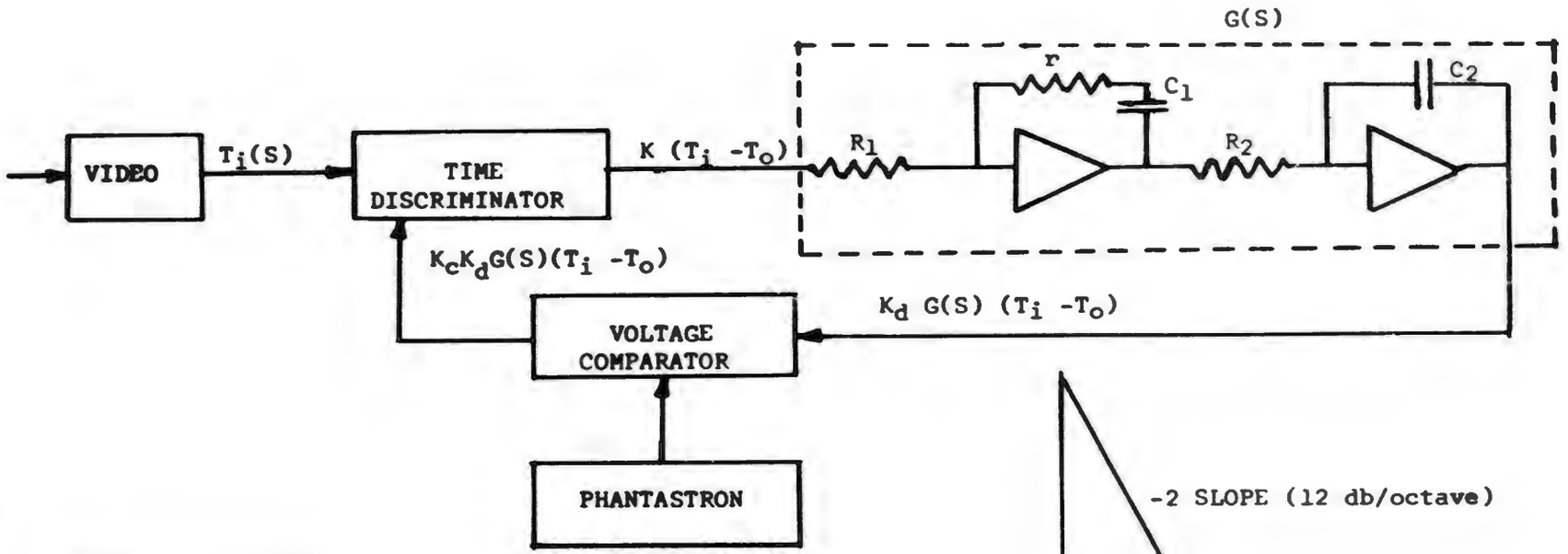

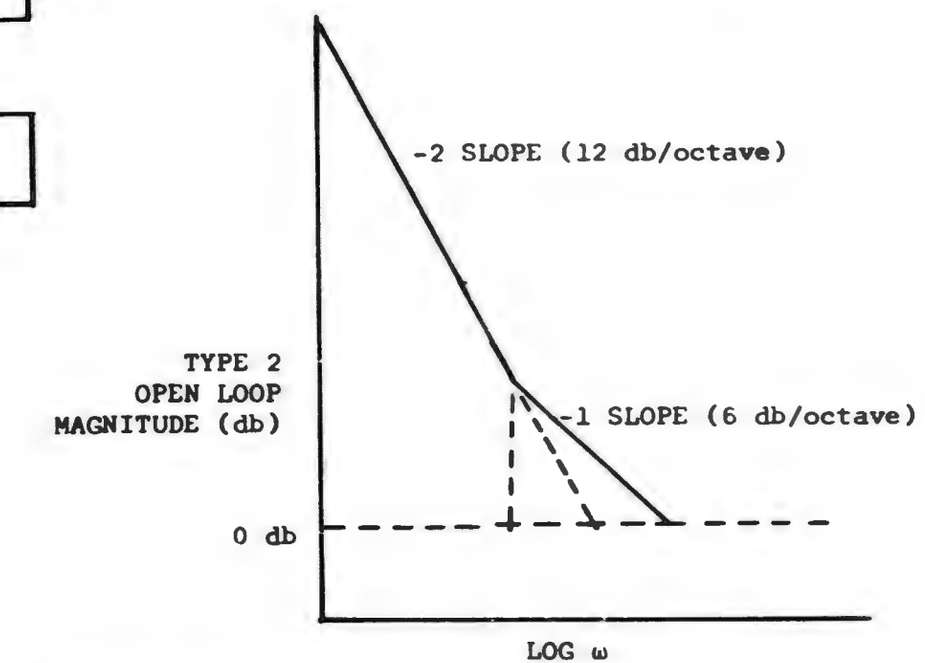

$$\frac{T_o(S)}{T_i(S)} = \frac{K_c K_d\, G(S)}{1 + K_c K_d\, G(S)}$$

$$G(S) = \frac{r}{R_1 R_2 C_2} \cdot \frac{S + 1/_r C_1}{S^2}$$

$$K = \frac{\omega_4}{\omega_3} = 2 = \frac{K_c K_d r^2 C_1}{R_1 R^2 C^2}$$

$$\omega_o = \omega_3 = \frac{1}{r C_1}$$

$$\omega_n = \omega_5$$

FIGURE 1 - TYPE 2 TRACKING LOOPS

3.0 Choice of Gein Factor

The choice of the gain factor is influenced by the contradictory requirements for good transient response and immunity to noise. The minimum noise bandwidth is obtained for K = 1. Reference to Figure 2 shows that the transient response is poor for K = 1. A good compromise is K = 2.

4.0 Corner Frequency (Angle Loop)

After arriving at a value for K, the corner frequency must be selected. It is obvious that the highest tracking loop bandwidth will be a function of the most severe target trajectory. This is the pass course depicted in Figure 3. It can be seen that

$$\theta = \tan^{-1} \frac{Vt}{R_o \cos \phi_o} \tag{5}$$

where V is target horizontal velocity
R_o is slant range at crossover
t is time
ϕ_o is target elevation angle at crossover.

The angular rates can be obtained by differentiating equation (5):

$$\ddot{\theta} = V \cos^2 \theta / R_o \cos \phi_o \tag{6}$$

$$\ddot{\theta} = -\left[\frac{V}{R_o \cos \phi_o}\right]^2 \cos^2 \theta \sin 2\theta \tag{7}$$

Both range and angle tracking loops are type 2 systems and consequently the system error expression is

$$\varepsilon(t) = \frac{\dddot{\theta}}{K\omega_o^2} - \frac{\ddot{\theta}}{K\omega_o^3} \qquad \text{.....} \tag{8a}$$

The error due to $\dddot{\theta}$ will not be considered since it is much smaller than $\ddot{\theta}$. Figure 4 is a comprehensive tabulation of the critical parameters involved in the choice of angle loop corner frequency (ω_o). A minimum range of five (5) miles with a maximum target velocity of 2000 ft/sec was selected. From information contained in Figure 4, it can be seen that a bandwidth (ω_o) of 1 radian will yield an error of

$$\varepsilon(t) \text{ max} = \frac{\dddot{\theta}}{K\omega_o^2} = \frac{2.83}{(2)\ (1)^2} \approx 1.4 \text{ milliradian} \tag{8b}$$

NOTES: FOR OVERDAMPED CASE, K > 4:

$$\theta_o(t) = 1 - \frac{K + \sqrt{K^2 - 4K}}{2\sqrt{K^2 - 4K}} \exp\left(K + \sqrt{K^2 - 4K}\right)\frac{\omega_o t}{2} + K - \sqrt{K^2 - 4K} \exp -\left(K - \sqrt{K^2 - 4K}\right)\frac{\omega_o t}{2}$$

FOR UNDERDAMPED CASE, K < 4:

$$\theta_o(t) = 1 + \frac{2}{4-K} \exp\left(-\frac{K\omega_o t}{2}\right) \sin\left(\sqrt{4K-K^2}\,\frac{\omega_o t}{2} - \tan^{-1}\frac{\sqrt{4 - K}}{K}\right)$$

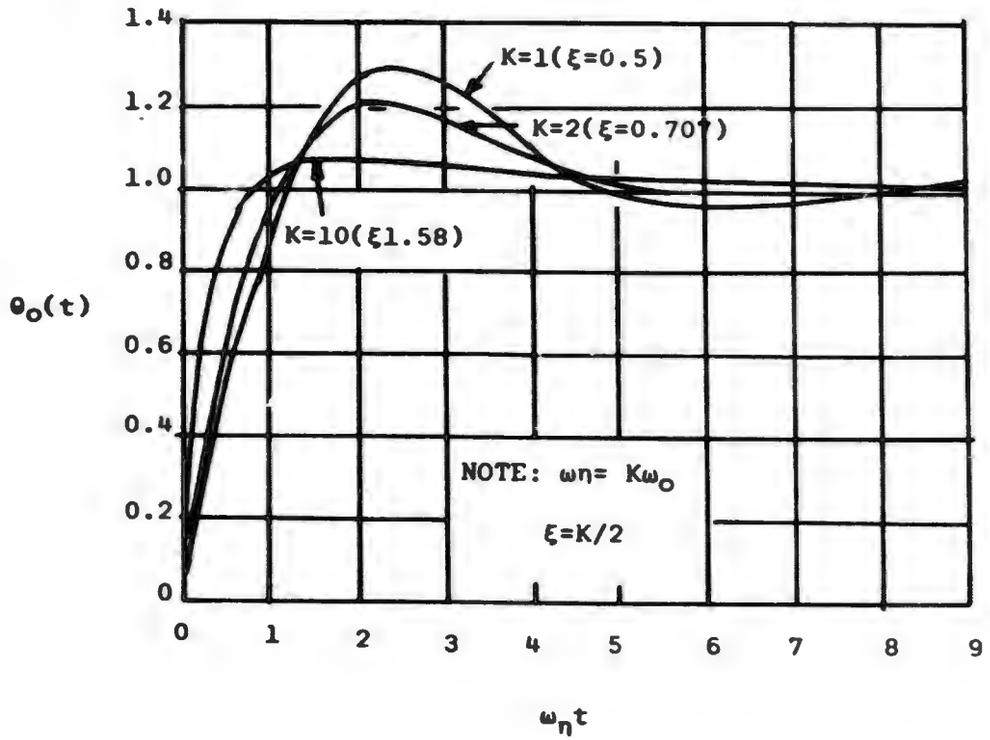

FIGURE 2 - TRANSIENT RESPONSE OF TYPE 2 SYSTEM FOR POSITION STEP INPUT

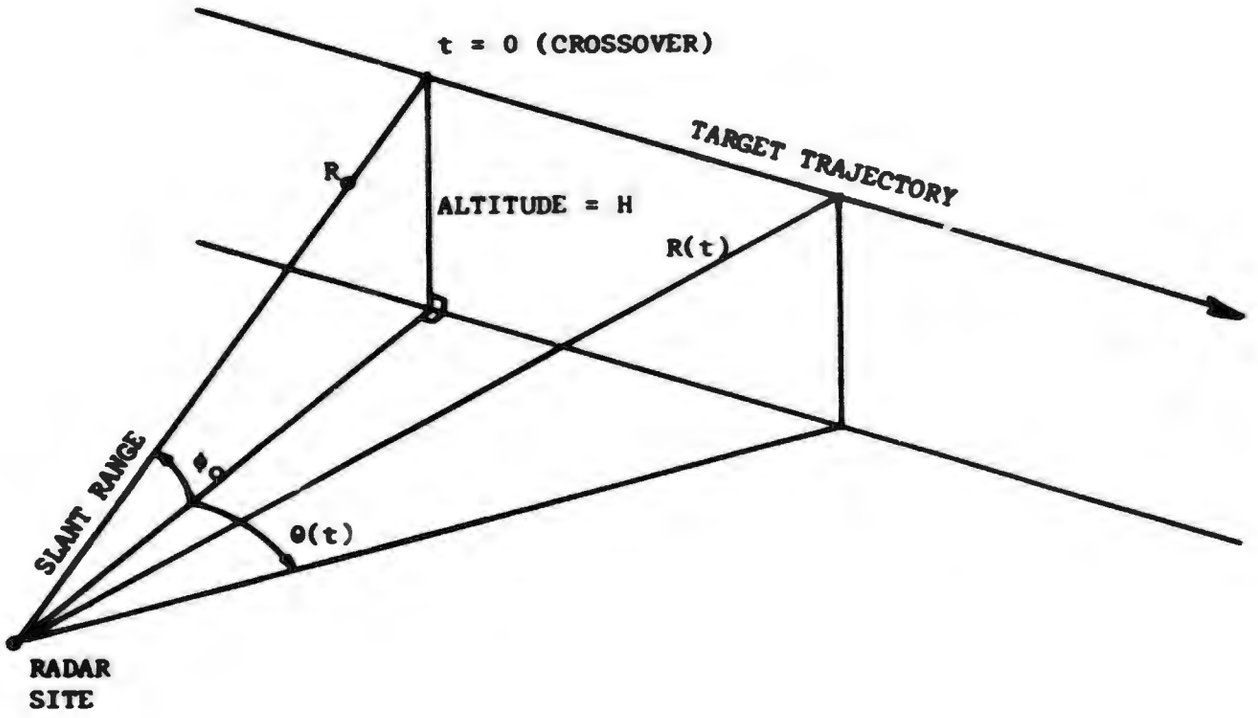

FIGURE 3 - PASS-COURSE TRACKING PROBLEM

Due to the lack of synchronization between prf and scan and also receiving system noise, it was felt that this bandwidth would result in noisy tracking and therefore should not be used unless necessary. Consequently, two somewhat arbitrary additional bandwidths were considered for slow, "and/or" long range targets. The medium and narrow bandwidths chosen were, respectively, .4 radian and .1 radian.

5.0 Selection of Components

Equation number (3) will be repeated at this time for convenience.

$$K = \frac{K_c K_d r^2 C_1}{R_1 R_2 C_2} = \frac{\omega_4}{\omega_3} = 2 \qquad (3)$$

Seven factors must be picked before equation (3) can be solved and two of these factors will vary to accomplish bandwidth selection. Since $\omega_o = 1/rC_1$, r will be switched rather than C_1. Due to a decision to keep K constant at 2, either R_1, R_2, or C_2 must be varied when ω_o is changed. This particular double integrator (see the G (S) block of figure 1) requires that R_1 be changed when r is changed. If R_2 or C_2 is changed while tracking any velocity (other than zero), the first integrator voltage will have to change at a prohibitive rate to accommodate the change in slope $\dot{\theta}/R_2C_2$ of the second integrator. Therefore, there is a problem with respect to loss of track. A far less serious problem exists with respect to acceleration when R_1 at input of the first integrator is suddenly changed. C_1 and C_2 are usually chosen with respect to memory considerations and physical size and .5 μf was selected. R_2 can be chosen arbitrarily, but due consideration must be given to the required dynamic range (Volts/Sec) at the output of the second or position integrator. R_2 = 3 megohms was chosen for the angle tracking loop.

6.0 Calculation of K_c and K_d (Angle Loops)

$$K_c = 50 \cdot 10^{-3}/200 = .25 \cdot 10^{-3} \text{ Sec/Volt.} \qquad (9)$$

K_d is equal to the discriminator output voltage divided by a tracking displacement (time).

$K \frac{(A-B)}{(A+B)}$ expresses the gain of the tracking loop discriminator

where (A-B) is the output voltage of the difference integrator and (A+B) is the output voltage of the sum integrator. Note that these voltages are a function of the time since they are derived from early and late gate coincidence circuitry. K is the voltage gain of the operational amplifiers within the Donner divider. An easy way to determine the gain (V/S) mathematically is to let the video (boxcar) be displaced with respect to the center of the tracking gate. Thus, if the width of the angle video is 5 ms, a misalignment of 2.5 ms will produce no output from one of the gates. Consequently, the output of the discriminator is $100 \cdot (A-0)/(A+0) = 100$ Volts and

TRACKING LOOP BANDWIDTH

LOOP	B. W. POSITION	ω_3	ω_5	ω_4
Angle	1	.1	.14	.2
Angle	2	.4	.56	.8
Angle	3	1.0	1.4	2.0
Range	1	.4	.56	.8
Range	2	1.0	1.4	2.0
Range	3	4.0	5.6	8.0

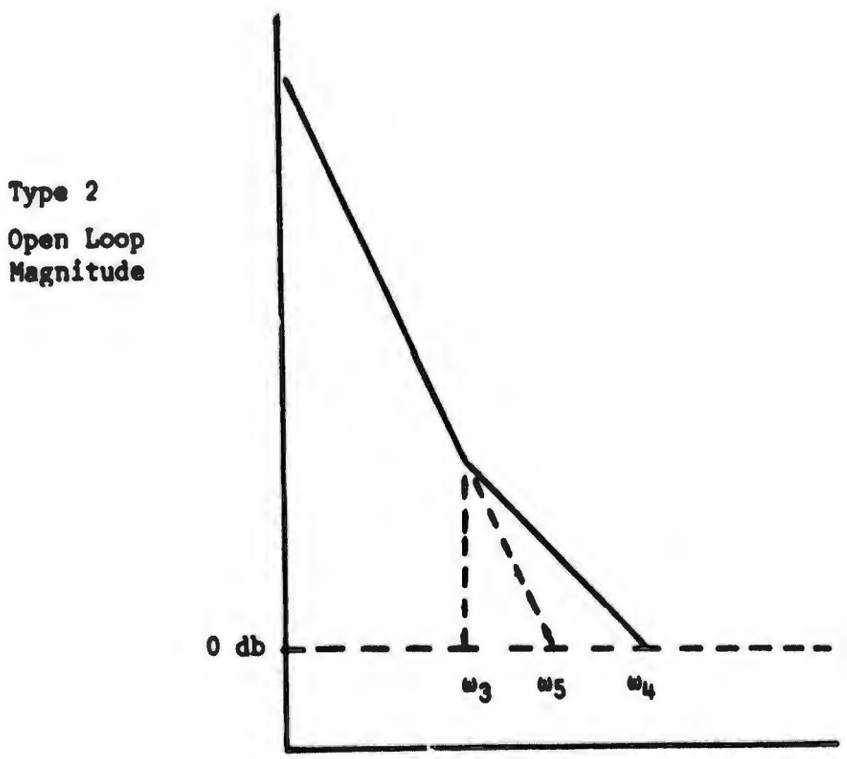

OPEN LOOP BANDWIDTH (RADIANS)

ω_3 Corner Frequency
ω_5 Natural Resonate Frequency (Undamped)
ω_4 Unity Gain Open Loop Frequency

FIGURE 4

$$K_d = 100/2.5 \cdot 10^{-3} = 40 \cdot 10^3 \text{ V/S} \tag{10}$$

hence

$$K_c K_d = (40 \cdot 10^3)\ (.25 \cdot 10^{-3}) = 10 \tag{11}$$

It is now possible to solve equation (3) for R_1 and the design of the angle tracking loop will be complete. A summary of the components making up equation (3) follows:

$$C_1 = C_2 = .5\ \mu f$$

$$\omega_o = \frac{1}{rC_1} = 1 \text{ radian}$$

$$r = \frac{1}{\omega_o C_1} = 2 \cdot 10^6 \text{ ohms}$$

$$R_2 = 3 \cdot 10^6 \text{ ohms}$$

$$K_c K_d = 10$$

$$R_1 = \frac{K_c K_d\ r^2 C_1}{K\ R_2 C_2} \tag{12a}$$

Consequently

$$R_1 = \frac{10 \cdot 4 \cdot 10^{12} \cdot\ .5 \cdot 10^{-6}}{2 \cdot 10^3 \cdot 10^6 \cdot\ .5 \cdot 10^{-6}} = 6.66 \text{ megohms} \tag{12b}$$

For bandwidths other than 1 radian, it is only necessary to solve for r and R_1 as shown above. The measured closed loop frequency response of the angle tracking loop is shown in Figure 5.

7.0 Range Tracking Loop Bandwidth

Except for a difference in bandwidth, K_c and K_d, the design of the range tracking loop, is similar to the design of the angle loop. Again, Figure 3 is used to determine the maximum rates for a pass course at five miles. Therefore,

$$R = R_o^2 + (Vt)^2\ 1/2 \tag{13}$$

and the range rates are

$$\dot{R} = \frac{V^2 t}{R_o^2 + (Vt)^2\ 1/2} \tag{14}$$

and

$$\ddot{R} = \frac{(VR_o)^2}{R_o^2 + (Vt)^2\ 3/2} \tag{15}$$

Figure 6 is a tabulation of ω_o required to produce acceptable tracking as a function of range and range rate. From the type 2 system error expression

$$\varepsilon = \frac{\ddot{R}}{(K\omega_o)^2} \tag{16}$$

hence

$$\omega_o = \frac{\ddot{R}}{K\varepsilon}\ 1/2 \tag{17a}$$

where

$R_o = 5$ NM

$\dot{R} = 132$ ft/Sec^2

$K = 2$

$\varepsilon = 10$ ft (arbitrarily selected)

$$\omega_o = \frac{132}{20}\ 1/2 = 2.57 \text{ radians} \tag{17b}$$

The above bandwidth will be troublesome with respect to lock-on for MACH 2 targets. Four radians is a good compromise between noise and acquisition of fast targets. Two additional bandwidths are provided as was done with the angle loops. These lower bandwidths are 1 radian and .4 radian. It is possible to track a MACH 2 target at five (5) miles (pass course) with a bandwidth of 1 radian. However, there will be 132/2=66 ft., which is .12μsec and dangerously close to the tracking gate width used in these calculations.

8.0 Calculation of K_c and K_d (Range Loops)

The comparator gain is

$$K_c = \frac{800 \cdot 10^{-6} \text{ Sec}}{200 \text{ Volts}} = 4.10^{-6} \text{ Sec/Volt} \tag{18}$$

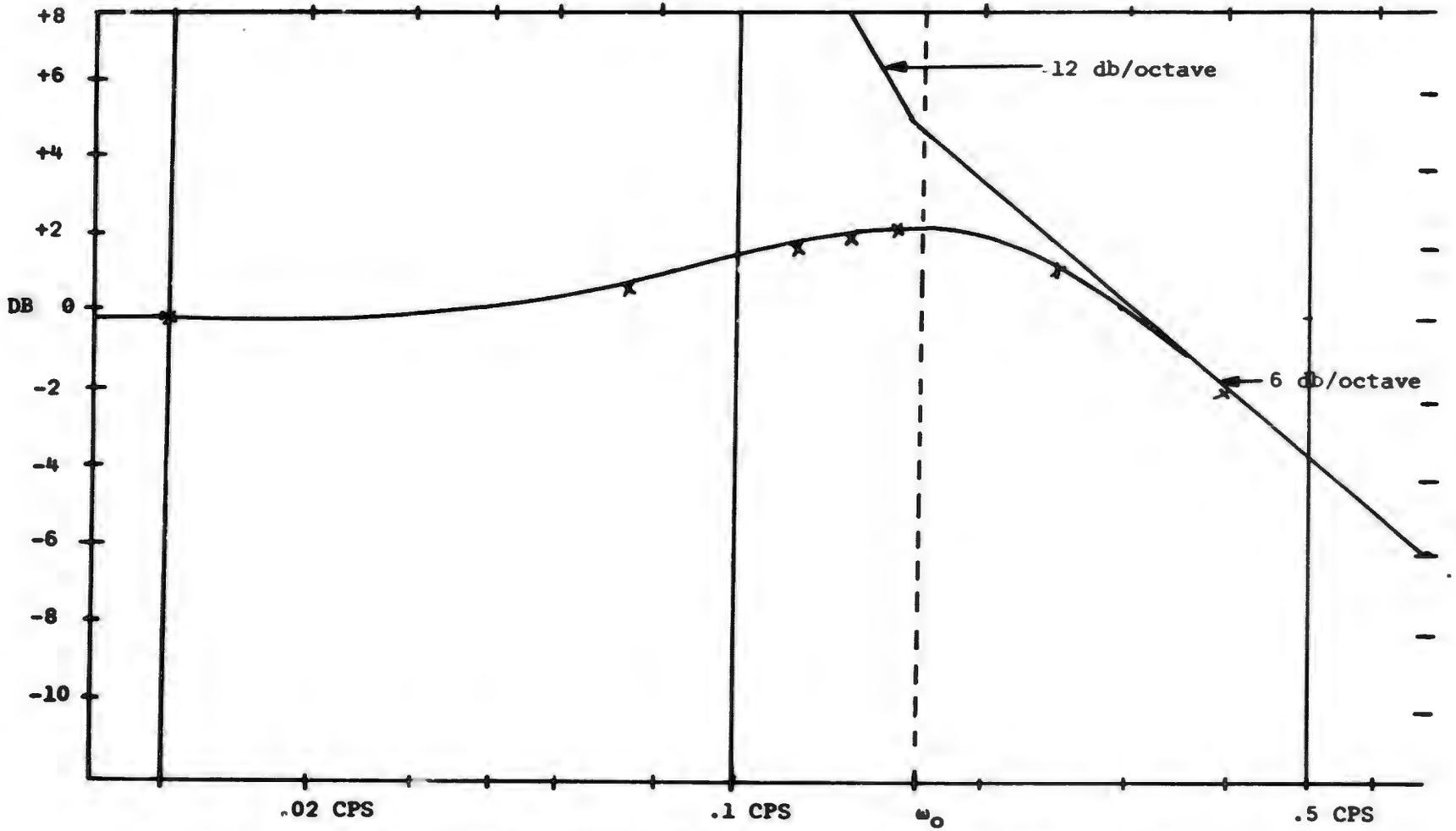

FIGURE 5 - FREQUENCY RESPONSE (ANGLE TRACKING LOOP ω_o = 1)

Since the discriminator gain varies with the video bandwidth, 0.5 μsec and 1.0 μsec were used. At low PRF's and at the 10 percent point it is very difficult to measure the gain (K_d); therefore, it was calculated as in the case of angle.

First, consider the .5 μsec. A misalignment of .5 μsec will produce no output from the late gate. Therefore, the output of the discriminator (which contains a divider whose output voltage can be expressed as)

$$E = (\Sigma A - \Sigma B) = 33 \text{ Volts } (B = 0)$$

Hence the gain V/S

$$K_d = 33 \text{ Volts}/.5 \cdot 10^{-6} \text{ Sec } (.1 \text{ μsec})$$

$$K_d = 33 \text{ Volts}/.25 \cdot 10^{-6} \text{ Sec } (.5 \text{ μsec})$$

$$K_c K_d = \frac{S}{V} \cdot \frac{V}{S} = 264 \ (.1 \text{ μsec})$$

$$K_c K_d = \frac{S}{V} \cdot \frac{V}{S} = 528 \ (.5 \text{ μsec})$$

To simplify the calculations, ... you can use the average gain ($K_c K_d$).

Therefore,

$$K_c K_d = \frac{528 + 264}{2} \approx 400 \tag{20}$$

Equation (3) will be solved again for R_1 which <u>must</u> be the variable when ω_o is changed. See Figure 1.

$$K = \frac{K_c K_d r^2 C_1}{R_1 R_2 C_2} \tag{3}$$

where

$K = 2$

$C_1 = C_2 = .5$ μf

$1/rC_1 = \omega_o = 4$ radians

$$r = \frac{1}{4 \cdot .5 \cdot 10^6} = .5 \cdot 10^6 \text{ ohms}$$

$R_2 = 20 \cdot 10^6$ ohms

Equation (3) can now be solved for R_1

$$R_1 = \frac{400 \cdot 25 \cdot 10^{10} \cdot .5 \cdot 10^{-6}}{2 \cdot 2 \cdot 10^7 \cdot .5 \cdot 10^{-6}} = 2.5 \cdot 10^6 \text{ ohms} \tag{21}$$

The measured frequency response of a range tracking loop is shown in Figure 7.

FIGURE 6 - CORNER FREQUENCY ω_o FOR $\ddot{R}_{max}$ AT VARIOUS RANGES AND VELOCITIES

$$\ddot{R} = \frac{V^2}{R_o} \cos\theta$$

$$\ddot{R}_{max} = \frac{V^2}{R_o}$$

$$\omega_o = \left[\frac{R}{2E}\right]^{1/2} \text{ radians}$$

$$\omega_o = \left[\frac{\ddot{R}}{2(30)}\right]^{1/2}$$

$$\omega_o = \left[\frac{\ddot{R}}{2(10)}\right]^{1/2}$$

$$\ddot{R} = \frac{V^2}{R_{o2}}$$

$R_{o_{nm}}$	R_o ft	V ft/sec	V^2 ft^2/sec^2	$\ddot{R}$ ft/sec	$\left[\ddot{R}\right]^{1/2}$	ω_o radians	ω_o
5	$3.03X10^4$	1000	$1X10^6$	33.1	5.76	0.744	1.28
10	$6.07X10^4$	1000	$1X10^6$	16.4	4.05	0.522	0.906
15	$9.1\ 10^4$	1000	$1X10^6$	11.1	3.34	0.431	0.745
20	$1.21X10^5$	1000	$1X10^6$	8.26	2.86	0.369	0.643
25	$1.52X10^5$	1000	$1X10^6$	6.58	2.56	0.330	0.573
30	$1.82X10^5$	1000	$1X10^6$	5.49	2.34	0.302	0.524
35	$2.12X10^5$	1000	$1X10^6$	4.71	2.18	0.281	0.486
40	$2.43X10^5$	1000	$1X10^6$	4.11	2.03	0.262	0.453
45	$2.74X10^5$	1000	$1X10^6$	3.64	1.91	0.246	0.421
50	$3.04X10^5$	1000	$1X10^6$	3.29	1.81	0.234	0.406
55	$3.34X10^5$	1000	$1X10^6$	2.99	1.73	0.223	0.387
60	$3.64X10^5$	1000	$1X10^6$	2.74	1.66	0.214	0.370
5	$3.03X10^4$	2000	$4X10^6$	132.0	11.5	1.48	2.57
10	$6.07X10^4$	2000	$4X10^6$	65.9	8.11	1.048	1.82
15	$9.11X10^4$	2000	$4X10^6$	53.9	6.62	0.854	1.48
20	$1.21X10^5$	2000	$4X10^6$	33.1	5.76	0.743	1.29
25	$1.52X10^5$	2000	$4X10^6$	26.3	5.14	0.665	1.15
30	$1.82X10^5$	2000	$4X10^6$	21.9	4.69	0.605	1.05
35	$2.12X10^5$	2000	$4X10^6$	18.9	4.35	0.561	0.974
40	$2.43X10^5$	2000	$4X10^6$	16.5	4.06	0.524	0.909
45	$2.74X10^5$	2000	$4X10^6$	14.6	3.82	0.493	0.854
50	$3.04X10^5$	2000	$4X10^6$	13.1	3.62	0.466	0.809
55	$3.04X10^5$	2000	$4X10^6$	12.0	3.46	0.446	0.775
60	$3.64X10^5$	2000	$4X10^6$	11.1	3.34	0.431	0.745

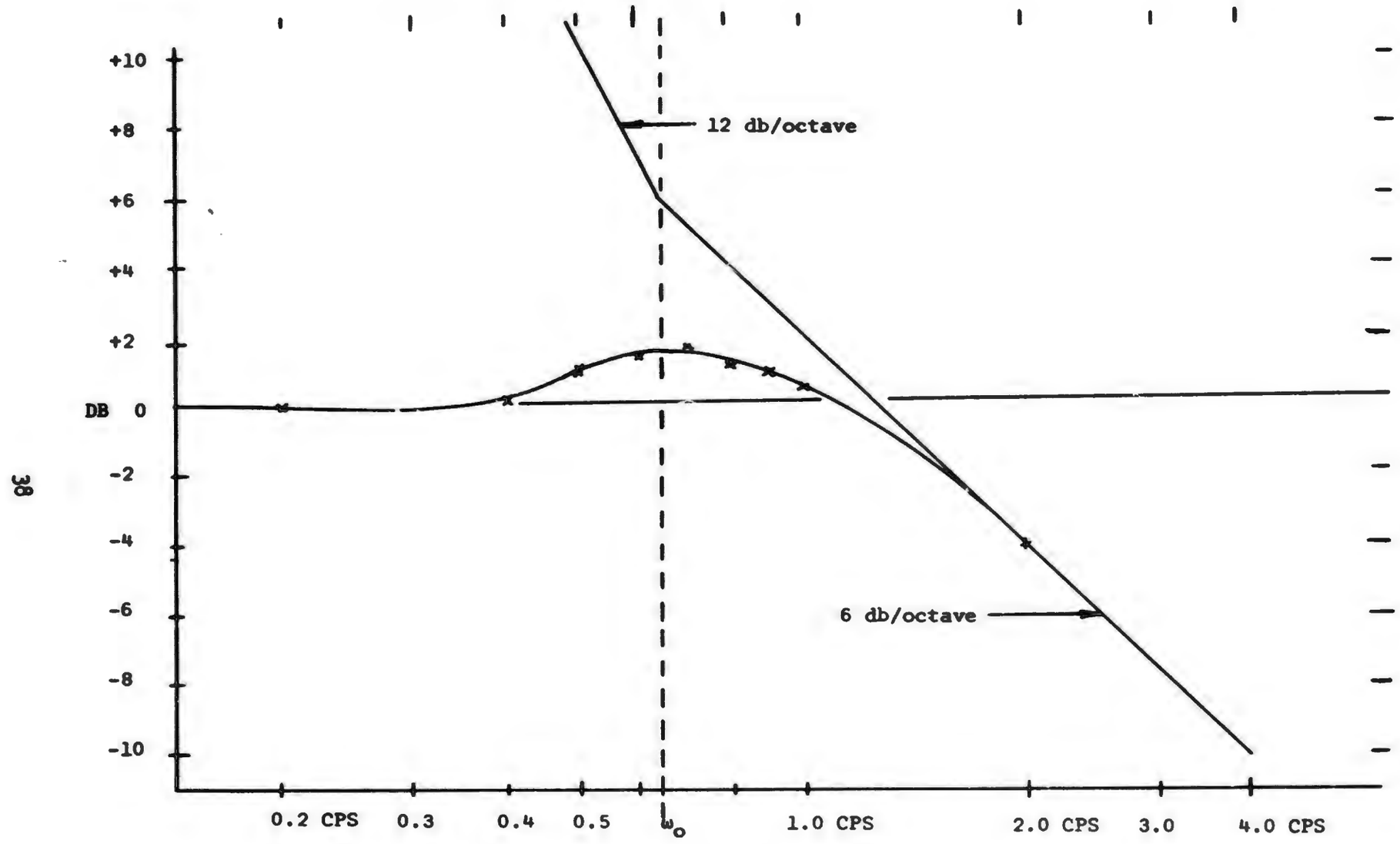

FIGURE 7 - FREQUENCY RESPONSE (RANGE TRACKING LOOP $\omega_o = 4$)

APPENDIX III

TRACKING LOOP ERRORS

TRACK-WHILE-SCAN

3.0 Tracking Loop Errors

The effect of the various radar parameters on the tracking accuracy of a track-while-scan radar has been theoretically analyzed by Swerling.[4] He has shown the lower bound of the variance of the angular position, estimate of a target is given by:

$$\sigma_{MIN}^2 = 0.239\ B\ \Delta\theta/X_o \tag{3.0}$$

where

σ_{MIN} = the lower bound of the standard deviation

B = the half power one-way antenna angular beam width (assumed Gaussian)

$\Delta\theta$ = angular distance between successive pulses emitted by the radar

X_o = signal-to-noise power ratio at the input to the second detectors, for a pulse emitted when the nose of the beam is pointing at the target (assumed to be much greater than unity).

The improvement in σ_{MIN} due to the integration of the tracking loop is shown for the case of a critically damped acceleration coupled servo to be

$$\sigma_{IMP} = \frac{\sigma_{MIN}}{\sqrt{.8\ \tau_s/T}} \tag{3.1}$$

where

σ_{IMP} = improved σ_{MIN}

τ_s = time constant of the servo

T = time between samples, i.e., reciprocal of scan rate

The actual operation of a track-while-scan system will suffer degradation since the assumptions made by Swerling are not met in practice. The beam is not Gaussian nor can one integrate without limit on both sides of the beam. If a sin x/x beam is assumed, integration can be performed from the beam center to where the beam gain has fallen to the vicinity of the side lobe level. Additionally, the beam shape information is analyzed by a split gate technique, and the question arises as to how close this split gate angle processor approaches the maximum likelihood detector of Swerling.

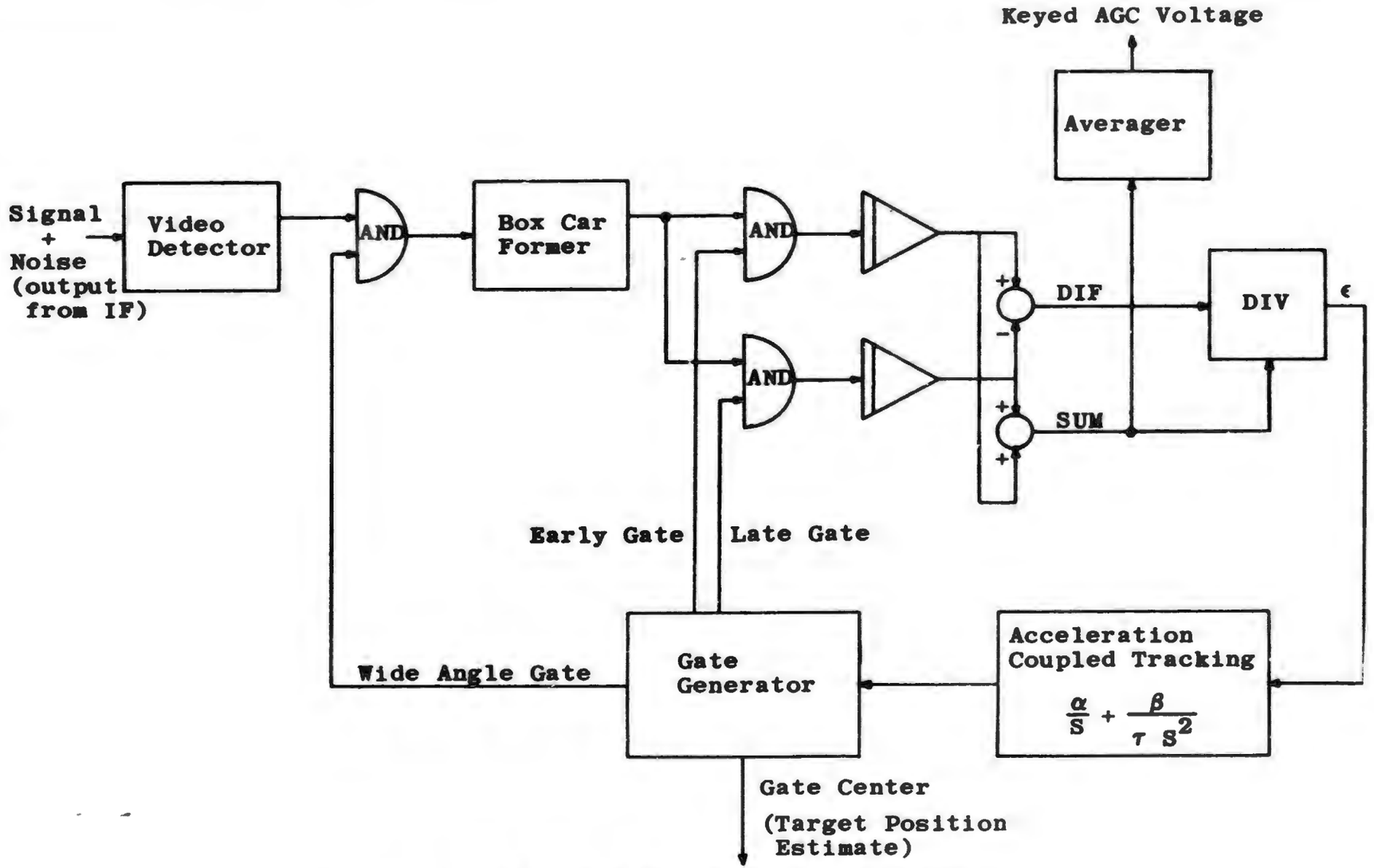

FIGURE 3.1 SPLIT GATE ANGULAR POSITION ESTIMATOR

A simulation of the split gate angle processor was designed. Figure 3.1 shows the block diagram. The output from the IF amplifier consists of gated signal pulses plus noise. For a perfect target reflector the IF signal has the form.

$$V = P \sin \omega t + N$$

where

V = IF output during a pulse

N = a noise voltage sloped mainly by the IF

ω = radian frequency of the IF

N can be considered to be made up of two components, N_p in phase with P and N_q in quadrative with P where the variance of N, N_p, and N_q are equal. The detector will process the envelope of this signal,

$$E(t) = \sqrt{(P + N_p)^2 + N_q^2} \tag{3.3}$$

and

$$\left(\frac{P}{\sigma_N}\right)^2 = X_o \tag{3.4}$$

where

E (t) is the envelope

p = the signal amplitude

σ_N = RMS noise voltage

X_o = signal-to-noise ratio

If the target is fluctuating, then V is given by

$$V = P_1 \sin \omega t + P_2 \cos \omega t + N \tag{3.5}$$

where P_1 and P_2 are from a gaussian distribution with variance σ_p

Then,

$$E(t) = \sqrt{(P_1 + N_p)^2 + (P_2 + N_q)^2} \tag{3.6}$$

and

$$\left(\frac{\sigma_p}{\sigma_N}\right)^2 = X_o \tag{3.7}$$

The amplitude of the signal varies during scan due to beam shape modulation. If the beam voltage distribution is sin x/x, then the voltage output will vary as $(\sin x/x)^2$; the square term arises from the modulation on both transmission and reception. When the wide angle gate is present, this signal passes through the AND gate and is box carred. Figures 3.2a, 3.2b, 3.2c and 3.2d show the process. The early and late gates, Figure 3.2e split the signal into two separate channels, Figures 3.2f and 3.2g. The signals are each integrated and the sum and difference formed. The sum is used to generate the AGC voltage for the IF. The difference, normalized by dividing by the sum, is the error signal which serves as the input to the acceleration coupled tracking loop with position smoothing constant, δ, and velocity smoothing constant, β. The output of the tracking loop is used to generate the wide angle gate, the early and late gates, and a pulse representing the center of the gates. This pulse represents the estimated angular position of the target.

It should be pointed out that as in Figure 3.2a, the beam does not necessarily point at the target at the time one of the pulses is emitted. This is due to the fact that the scan rate and PRF are not necessarily synchronized. The assumption can be made that over a large number of sweeps, the true target position is uniformly distributed over the interval between pulses. This was verified by computer runs and introduces negligible error as long as $\sigma_{MIN} > \frac{\Delta\theta}{10}$ A second error exists in which the box carring will bias the target half a pulse width in the direction of the late gate. Error compensation can be applied to remove this bias. A third error is induced by the beam shape $\frac{\sin x}{x} \cdot \frac{\sin (x + \Delta x)}{x + \Delta x}$. The first of these last two bias errors is corrected in the analysis; the last is ignored.

It is convenient to define several parameters. If B is the beam width as defined in Equation 3.0,

$$P_W = 100\ W/.5B \tag{3.8}$$

$$P_S = 100\ S/.5B \tag{3.9}$$

where

W = Half gate width
S = Half gate separation
P_W = Half gate width in % half beam widths
P_S = Half gate separation in % half beam widths

The analysis was checked by using an exponential beam and a value of $P_B = 0$ and $P_W = 400$. This amounts to integrating 99 percent of the exponential beam. The open loop standard deviation agreed with Equation 3.0 to within 1 to 2 DB and the closed loop performance yielded an improvement predicted by Equation 3.1. With the simulation working, the exponential beam was replaced by a $(\sin x/x)^2$ beam. The difference in these two beam shapes can be seen in Figure 3.3. For the purpose of the analysis, the side lobe level of the

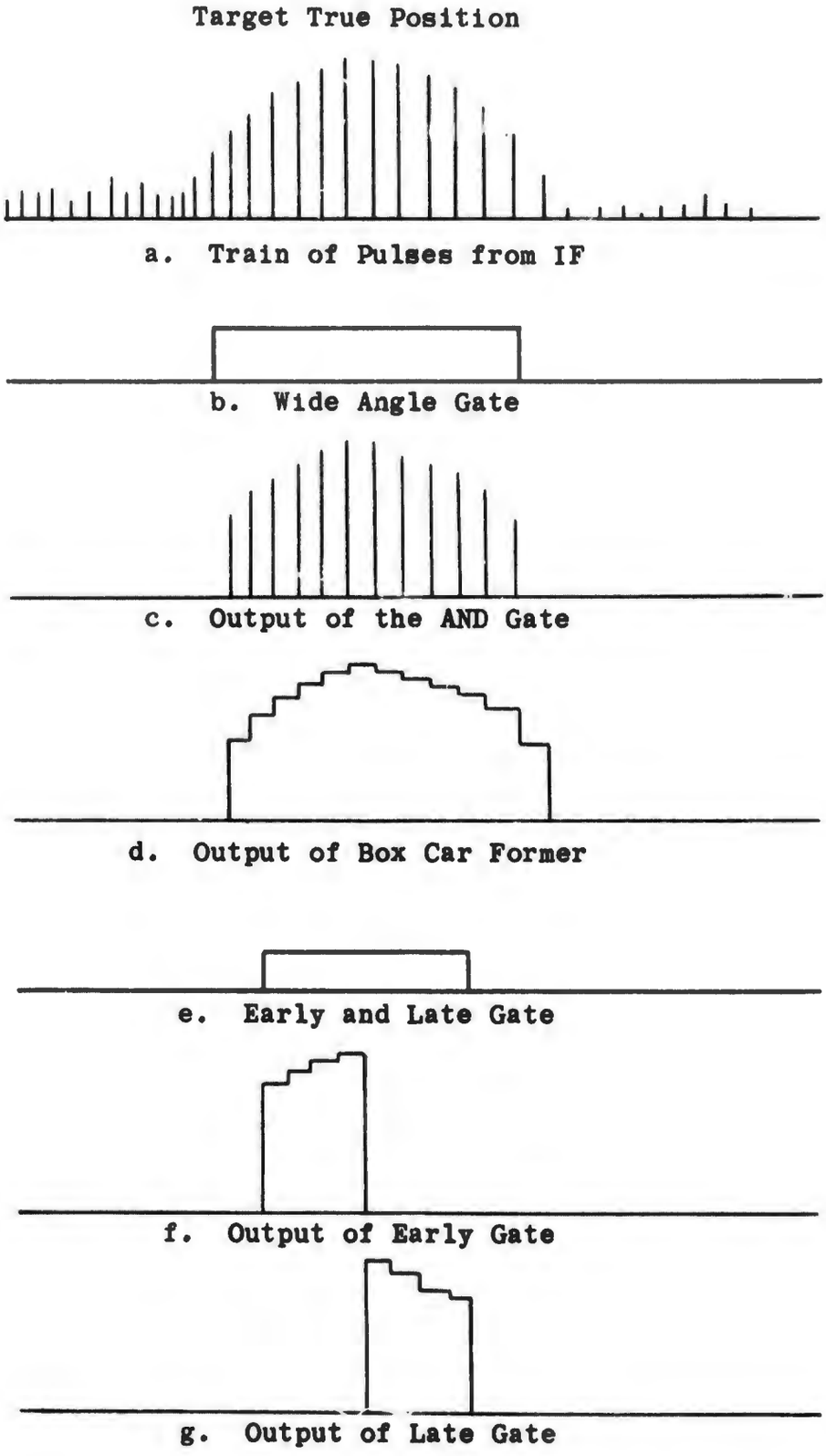

FIGURE 3.2 SKETCH SHOWING THE SIGNAL PROCESSING IN THE TRACKING LOOP

$(\sin x/x)^2$ beam was assumed to be constant at 16 DB down. In practice, any beam processing would nominally stop short of the expected side lobe structure. A level of -13 DB would probably be reasonable.

To test the split gate "Pant Leg" gate technique of P_w from 20% to 200% and values of P_s from 0 to 100% were used. It should be pointed out that these values of P_w and P_s are constrained. Since the -13 DB level will occur at 181% of the half beam width point,

$$P_w + P_s \geq 181\% \tag{4.0}$$

A signal-to-noise ratio of 10 DB and a $\Delta\theta/B$ ratio of approximately 0.1 was used. The results are shown in Figure 3.4. The effect of the constraint is to produce a minimum in the normalized $\sigma^2/B\ \Delta\theta$ curve. Thus, with a $P_w = 115\%$ and a $P_s = 66\%$, the best tracking accuracy is attained. The point labeled (A) in Figure 3.4 shows the location of the parameters of the gates. The values are $P_w = 118\%$ and $P_s = 59\%$, and were used in the subsequent analysis.

A sensitivity study was made to determine the effect of the signal-to-noise ratio, X_o. Values of X_o from 1.0 to 100 were used. Both scan-to-scan fluctuating and non-fluctuating targets were assumed. Thus, equations 3.4 and 3.5 for the fluctuating case or 3.6 and 3.7 for the non-fluctuating cases are used. By scan-to-scan fluctuation, it is implied that the radar cross section is varying in a random fashion, slow enough that it can be considered constant while the N pulses are received during a single scan, but is fast enough to produce independent values from scan-to-scan. In the case of jet aircraft, this condition is met. For the non-fluctuating case, Equation 3.0 implies a dependence of the normalized parameter $\sigma^2/B\ \Delta\theta$ on the inverse of the signal-to-noise ratio. The lower curve of Figure 3.5 shows the results of the analysis. The upper curve is for the fluctuating target case. For the purpose of analyzing the effect of tracking accuracy, an empirical relationship expressing the dotted curve will be used, namely.

$$\sigma_{MIN}{}^2 = 1.34\ B\ \Delta\theta\ X_o^{-.7} \tag{4.1}$$

This equation implies that σ_{MIN} is directly proportional to the $B\ \Delta\theta$ product and is only indirectly sensitive to the number of pulses processed. However, if $B = 1°$ and $\Delta\theta = 1°$, the optimum half gate width as obtained from Equation 3.8 with $P_w = 115$ percent is

$$\begin{aligned} W &= 0.5\ B\ (P_w)/100 \\ &= 0.5\ (1°)\ (115)/100 \\ &= 0.525° \end{aligned} \tag{4.2}$$

The total gate width is then $2\ (0.525) = 1.15°$ implying only one pulse is available for processing by the split gate. This obviously places a limit on the usability of the equation. Various $\Delta\theta$, B combinations were analyzed.

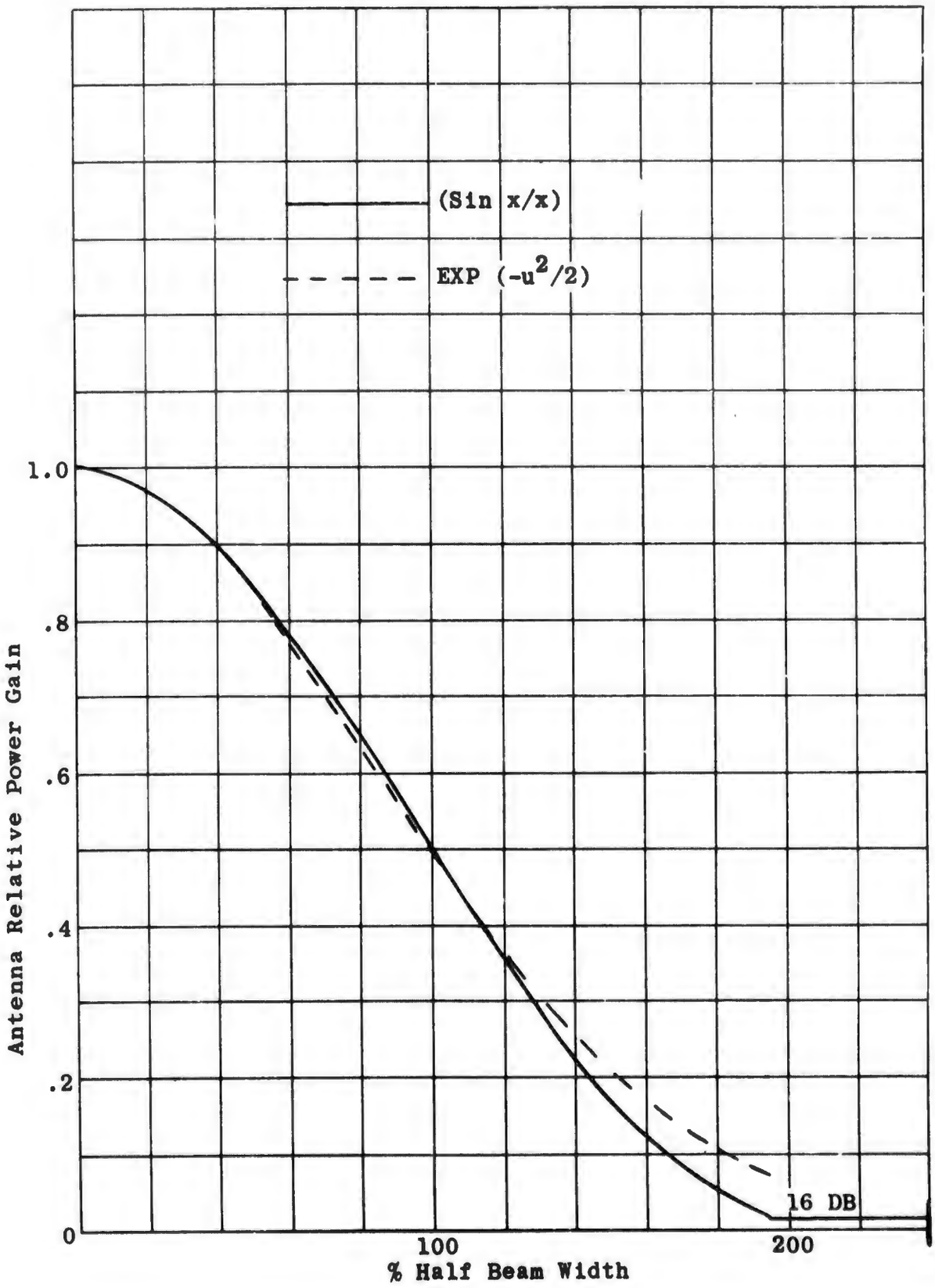

FIGURE 3.3 ANTENNA BEAM SHAPE USED IN THE TRACKING LOOP

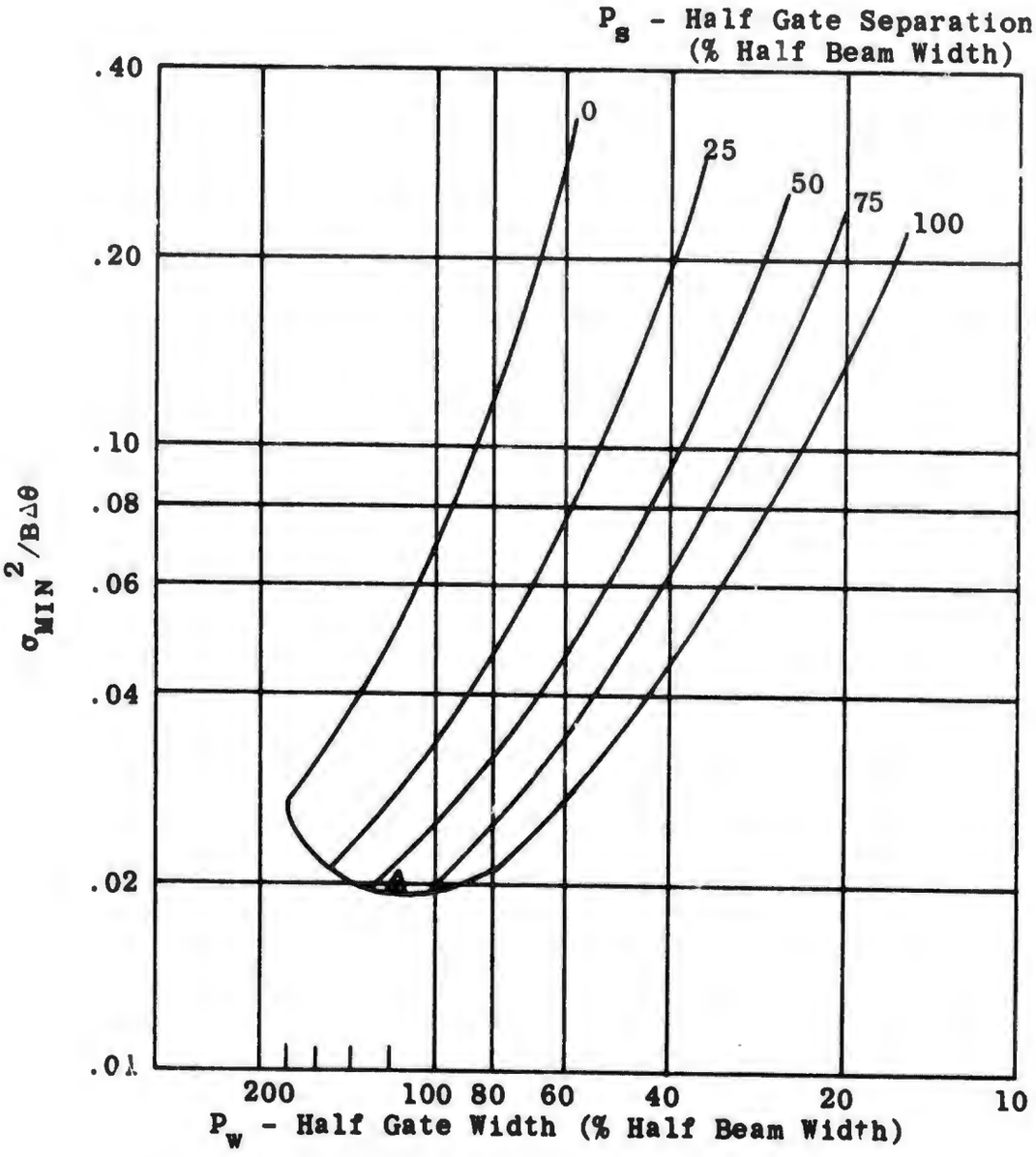

FIGURE 3.4 EFFECT OF "PANT LEG" GATE PARAMETERS ON NORMALIZED TRACKING ACCURACY FOR SCAN ON BOTH TRANSMIT AND RECEIVE

The results are shown in Figure 3.6. The parameter Λ is a factor by which Equation 4.2 should be multiplied to include this dependency on the number of pulses, thus

$$\sigma_{MIN}^2 = .134\ B\ \Delta\theta\ \Lambda\ X_o^{-.7} \tag{4.3}$$

and from Figure 3.4

$$\Lambda = .5\ \frac{(\Delta\theta)}{B} = .3 \tag{4.4}$$

Combining Equations 4.3 and 4.4 and rearranging terms

$$\sigma_{MIN}^2 = 0.067\ B^2\ \left(\frac{\Delta\theta}{B}\ .\frac{1}{X_o}\right)\ 0.7 \tag{4.5}$$

A further effect is present as $\Delta\theta$ becomes large. This is due to the lack of synchronism between the PRF and scan rate producing an apparent target location uniformly distributed over the range $\Delta\theta$. As previously described, the influence on $\sigma_{MIN} > \frac{\Delta\theta}{10}$. Actually, the value $\frac{\Delta\theta}{10}$ should be added (RMS) to all calculated values of $\sigma_{MIN} > \Delta\theta$ to include the contribution of apparent target distribution. Thus, Equation (4.5) should be written as

$$\sigma_{MIN}^2 = 0.067\ B^2\ \left(\frac{\Delta\theta}{B}\ .\ \frac{1}{X_o}\right)^{0.7} + \frac{(\Delta\theta)^2}{10} \tag{4.6}$$

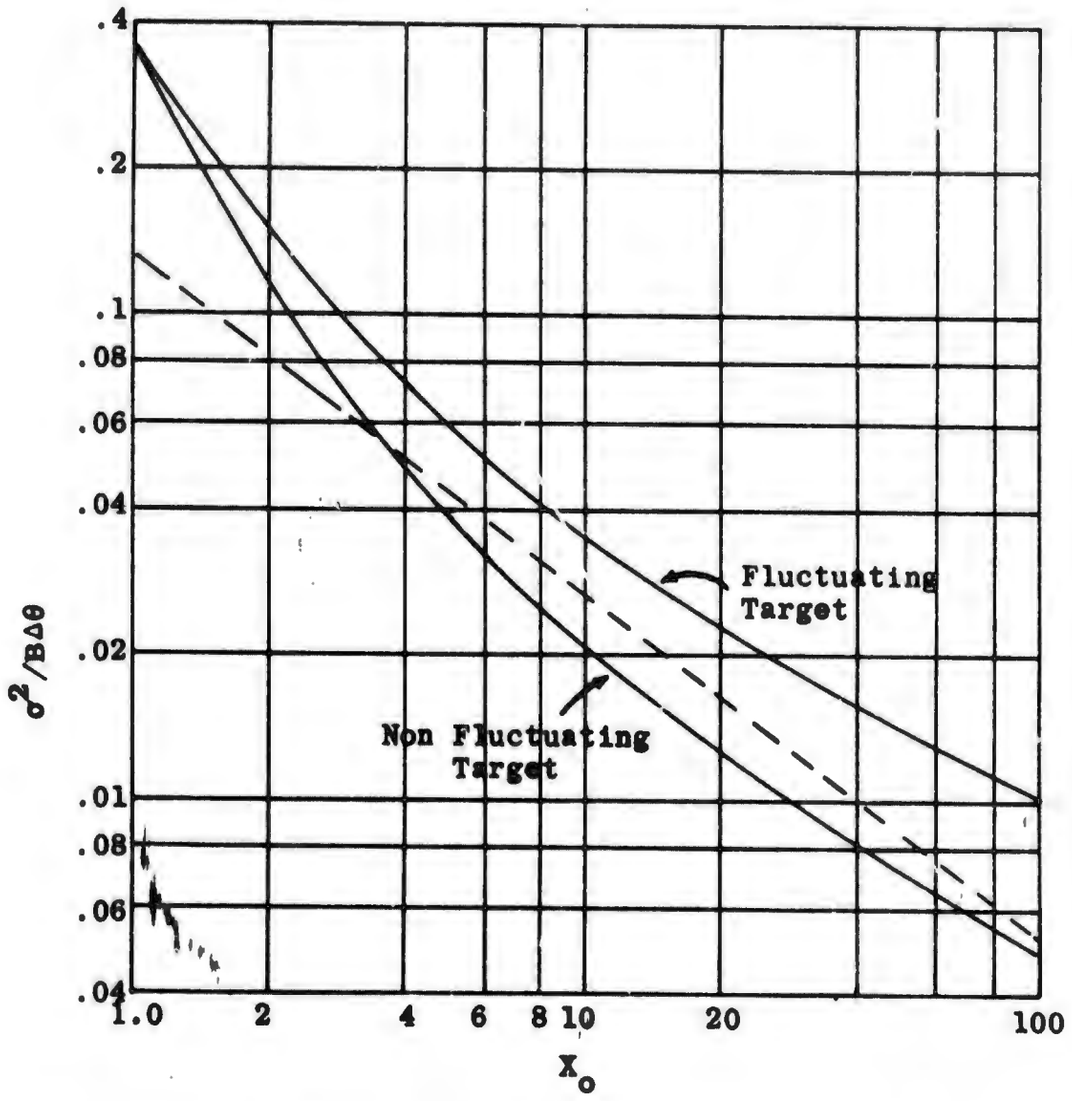

FIGURE 3.5 EFFECT OF SIGNAL-TO-NOISE RATIO ON TRACKING ACCURACY

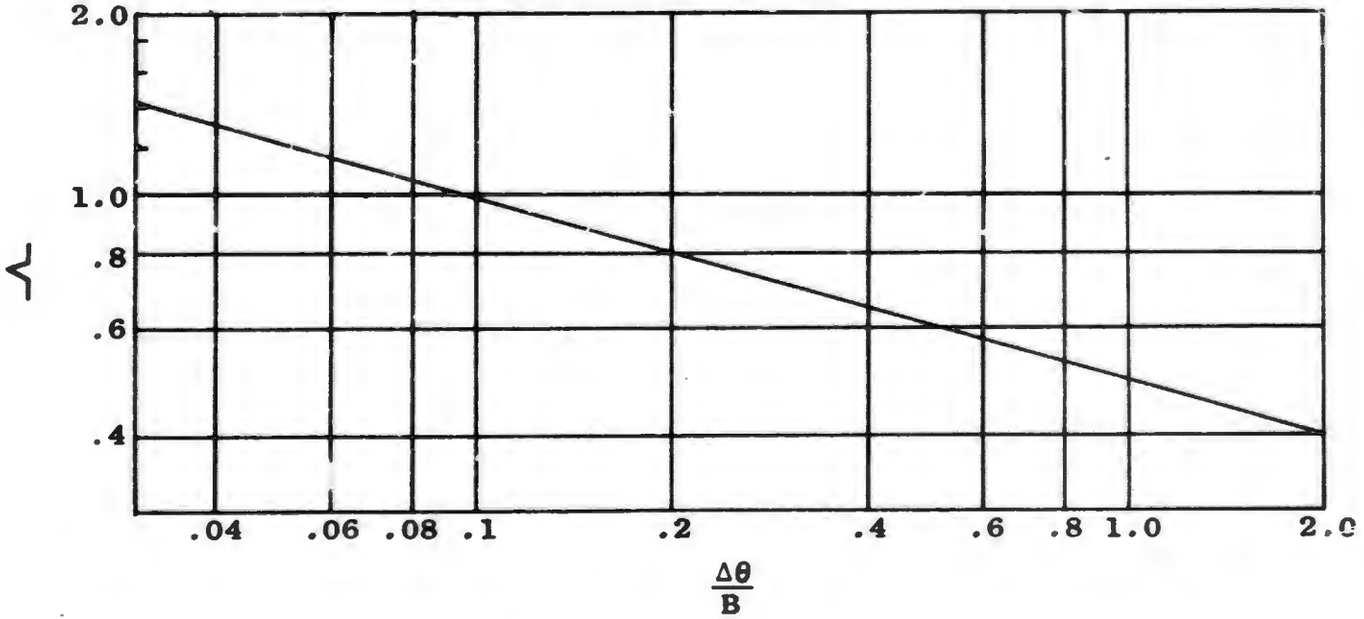

FIGURE 3.6 PULSE PROCESSING EFFICIENCY

LIST OF REFERENCES

1. Barton, David - "Radar System Analysis" Prentice-Hall, 1964.

2. Berkowitz, Raymond - "Modern Radar Analysis Evaluation and System Design" Wiley and Son, 1965.

3. Skolnick, Merrill - "Introduction to Radar Systems" McGraw Hill, 1962.

4. Swerling, Peter - "Probability of Detection for Fluctuating Targets" Rand Corporation, Research Memo RM-1217 March 1954 (Proceedings IRE-IT-6, No. 2, April 1960).

5. Final Report - "Instrumentation Radar, AN/FPS-16(XN-2)" - AD 250 500 RCA Defense Electronics Product (Moorestown) - Contract - Navy

6. Final Report, Classified Secret - "(U) Simulated Air Defense System MOD I" RADC-TR-66-390 - AD 382 412L.

7. Final Report, Classified Secret - "(U) Simulated Air Defense System MOD II" RADC-TR-65-342 - AD 372 170L.

LIST OF ABBREVIATIONS AND SYMBOLS

(NOTE: Only those not defined where used, are listed)

AGC - Automatic Gain Control

ATR - Anti-Transmit-Receive

AZ - Azimuth

BW - Bandwidth

DB - Decibel

EL - Elevation

IF - Intermediate-Frequency

LO - Local Oscillator

PRF - Pulse Repetition Frequency

NM - Nautical Miles

RF - Radio Frequency

TR - Transmit Receive

Σ - Summation or Sum

Δ - Difference

μ - Micro

ω - Frequency (Radians)

MACH - Ratio of Flight Speed to Speed of Sound

UNCLASSIFIED

Security Classification

DOCUMENT CONTROL DATA - R & D

(Security classification of title, body of abstract and indexing annotation must be entered when the overall report is classified)

1 ORIGINATING ACTIVITY (Corporate author)
Rome Air Development Center (EMCVM-4)
Griffiss Air Force Base, N.Y.

2a. REPORT SECURITY CLASSIFICATION
UNCLASSIFIED

2b GROUP

3 REPORT TITLE
COMPARISON OF MONOPULSE AND MECHANICAL TRACK-WHILE-SCAN RADARS

4. DESCRIPTIVE NOTES (Type of report and inclusive dates)
Final In-house

5 AUTHOR(S) (First name, middle initial, last name)
Charles F. Bough

6 REPORT DATE
May 1968

7a. TOTAL NO OF PAGES
54

7b. NO OF REFS
7

8a. CONTRACT OR GRANT NO

b. PROJECT NO. 4557

c.

d.

9a. ORIGINATOR'S REPORT NUMBER(S)
RADC-TR-68-125

9b. OTHER REPORT NO(S) (Any other numbers that may be assigned this report)

10 DISTRIBUTION STATEMENT
This document is subject to special export controls and each transmittal to foreign governments, foreign nationals, or representative thereto may be made only with prior approval of RADC (EMCVM-4), GAFB, N.Y. 13440.

11. SUPPLEMENTARY NOTES

12. SPONSORING MILITARY ACTIVITY
Rome Air Development Center (EMCVM-4)
Griffiss AFB, N.Y. 13440.

13 ABSTRACT
7 This report compares the angle-range tracking capabilities of amplitude monopulse radars and track-while-scan radar using mechanical scanners developed by Lewis (U.S. Patent No. 2,585,562). Both systems are described along with an error analysis of the angle-range tracking loops. A table is included which summarizes the characteristics of the two systems.

DD FORM 1 NOV 68 1473

UNCLASSIFIED

Security Classification

14 KEY WORDS	LINK A		LINK B		LINK C	
	ROLE	WT	ROLE	WT	ROLE	WT
Radar, Surveillance, Tracker, Instrumentation Radar Detection, Radar Scanning						

UNCLASSIFIED

AD 833249/RADC-TR-68-125, May 1968
Comparison of Monopulse and Mechanical Track-While-Scan

ERRATA - July 1969

Attached page 47 is to be permanently affixed over the existing page 47 in RADC-TR-68-125.

Rome Air Development Center
Air Force Systems Command
Griffiss Air Force Base, New York

The results are shown in Figure 3.6. The parameter Λ is a factor by which Equation 4.2 should be multiplied to include this dependency on the number of pulses, thus

$$\sigma_{MIN}^2 = .134\ B\ \Delta\theta\ \Lambda\ X_0^{-0.7} \tag{4.3}$$

and from Figure 3.4

$$\Lambda = .5\left[\frac{\Delta\theta}{B}\right]^{-0.3} \tag{4.4}$$

Combining Equations 4.3 and 4.4 and rearranging terms

$$\sigma_{MIN}^2 = 0.067\ B^2\left[\frac{\Delta\theta}{B}\cdot\frac{1}{X_0}\right]^{0.7} \tag{4.5}$$

A further effect is present as $\Delta\theta$ becomes large. This is due to the lack of synchronism between the PRF and scan rate producing an apparent target location uniformly distributed over the range $\Delta\theta$. As previously described, the influence on $\sigma_{MIN} > \frac{\Delta\theta}{10}$. Actually, the value $\frac{\Delta\theta}{10}$ should be added (RMS) to all calculated values of $\sigma_{MIN} > \Delta\theta$ to include the contribution of apparent target distribution. Thus, Equation (4.5) should be written as

$$\sigma_{MIN}^2 = 0.067\ B^2\left[\frac{\Delta\theta}{B}\cdot\frac{1}{X_0}\right]^{0.7} + \frac{(\Delta\theta)^2}{10} \tag{4.6}$$